Am J Physiol Lung Cell Mol Physiol 316: L723–L737, 2019.
First published January 17, 2019; doi:10.1152/ajplung.00058.2018.

RESEARCH ARTICLE

Mesenchymal stromal cell-derived exosomes improve mitochondrial health in pulmonary arterial hypertension

Sarah E. Hogan,* Maria Pia Rodriguez Salazar,* John Cheadle, Rachel Glenn, Carolina Medrano, Thomas H. Petersen, and Roger M. Ilagan

Department of Regenerative Medicine, United Therapeutics Corporation, Durham, North Carolina

Submitted 5 February 2018; accepted in final form 7 January 2019

Hogan SE, Rodriguez Salazar MP, Cheadle J, Glenn R, Medrano C, Petersen TH, Ilagan RM. Mesenchymal stromal cell-derived exosomes improve mitochondrial health in pulmonary arterial hypertension. *Am J Physiol Lung Cell Mol Physiol* 316: L723–L737, 2019. First published January 17, 2019; doi:10.1152/ajplung.00058.2018.—Secreted exosomes are bioactive particles that elicit profound responses in target cells. Using targeted metabolomics and global microarray analysis, we identified a role of exosomes in promoting mitochondrial function in the context of pulmonary arterial hypertension (PAH). Whereas chronic hypoxia results in a glycolytic shift in pulmonary artery smooth muscle cells (PASMCs), exosomes restore energy balance and improve O_2 consumption. These results were confirmed in a hypoxia-induced mouse model and a semaxanib/hypoxia rat model of PAH wherein exosomes improved the mitochondrial dysfunction associated with disease. Importantly, exosome exposure increased PASMC expression of pyruvate dehydrogenase (PDH) and glutamate dehydrogenase 1 (GLUD1), linking exosome treatment to the TCA cycle. Furthermore, we show that although prolonged hypoxia induced sirtuin 4 expression, an upstream inhibitor of both GLUD1 and PDH, exosomes reduced its expression. These data provide direct evidence of an exosome-mediated improvement in mitochondrial function and contribute new insights into the therapeutic potential of exosomes in PAH.

exosome; glutamate dehydrogenase; glycolysis; hypertension; hypoxia; pulmonary; pyruvate dehydrogenase; sirtuin 4; tricarboxylic acid cycle

INTRODUCTION

Pulmonary arterial hypertension (PAH), a vascular remodeling disease of the lungs, results in increased pulmonary vascular resistance leading to right ventricular failure. Excessive proliferation and impaired apoptosis of pulmonary artery (PA) smooth muscle cells (PASMCs) are thought to be key contributors to the remodeling associated with PAH (33, 41). Despite the availability of therapies that improve the symptoms of PAH and major advances in our understanding of molecular mechanisms that underlie vascular remodeling, a cure for the disease has yet to be identified. Emerging evidence suggests that abnormalities exist in multiple organ systems (heart, skeletal muscle, and spleen), all of which contribute to the pathogenesis of PAH (4, 44). Therefore, current therapies focused on lung architecture may fail to treat all complexities of the disease. The finding that PAH is a metabolic disease could provide a unifying model to explain phenotypic similarities in diseased cells from multiple tissues.

Insulin resistance and glucose intolerance, secondary to mitochondrial dysfunction, have been shown to correlate with PAH pathogenesis (1, 5, 66). Similar to a cancerous phenotype, PAH-associated cells undergo a metabolic shift toward glycolysis and lactic acid fermentation, which enables sustained ATP production and uncontrolled cellular growth (45). The resulting hyperproliferation and resistance to apoptosis complexes with aberrant mitochondrial function in the form of diminished glucose oxidation, anaplerosis into the TCA cycle, and oxidative phosphorylation (12, 16, 49, 51). Because these abnormalities are thought to precede disease progression in PAH, therapeutic targeting of mitochondrial dysregulation could provide an avenue into disease prevention or reversal (23). Although several strategies for targeting the metabolic aspects of PAH have been proposed (56), a multifaceted approach may be required to combat the underlying metabolic causes, in addition to regeneration of lung microvasculature.

Stem cell therapy has emerged as a promising strategy for the treatment of PAH (54). However, stem cell transplants are often complicated by graft-versus-host concerns (28). Further studies determined that paracrine signaling in the form of exosomes could harness the benefits of stem cell therapy while avoiding transplantation-induced complications (64). Indeed, promising work has described an exosome-mediated reversal of the pulmonary arterial muscularization and right ventricular hypertrophy associated with PAH (22, 31). Because emerging evidence suggests that exosomes contain mitochondrial material (30, 46, 62), we hypothesized that they could have a previously unidentified role in the promotion of mitochondrial function within the context of PAH.

Herein, we sought to determine whether mesenchymal stromal cell (MSC)-derived exosomes could improve the mitochondrial deficit in PAH. To that end, we examined the impact of exosomes on mitochondrial health in PASMCs after a chronic hypoxia exposure and in a semaxanib/hypoxia rat model of PAH. Our findings establish an important role for exosomes in increasing metabolic flux into the TCA cycle through regulation of the sirtuin 4 (SIRT4) signaling pathways, thus improving mitochondrial function. These data suggest that exosomes function to improve the underlying metabolic dysfunction associated with PAH.

* S. E. Hogan and M. P. R. Salazar contributed equally to this article.

Address for reprint requests and other correspondence: S. E. Hogan, United Therapeutics Corp., 55 TW Alexander Dr., Durham, NC 27709 (e-mail: sseiler@unither.com).

METHODS

Preparation of exosomes. Primary human bone marrow-derived mesenchymal stromal cells (MSCs; RoosterBio) were cultured as previously described (31). In brief, MSCs were grown in KT-001 growth media (RoosterBio) until 100% confluent. Cells were then washed twice with PBS and incubated in serum-free, protein-free basal media for 48 h. Conditioned media was collected, filtered (0.2 μm filter), and adjusted to 10 mM EDTA and 25 mM HEPES. Conditioned media was concentrated by tangential flow filtration (Sartorius), and exosomes were purified using a size exclusion column packed with Sepharose CL-2B resin (GE Healthcare). In-line A280 wavelength data collection and choline-containing phospholipids such as lecithin, lysolecithin, and sphingomyelin (Phospholipid Assay Kit, Sigma) were measured and used to identify and pool the exosome-containing fractions.

Exosome antibody array. Exosomes were examined for known exosome markers flotillin-1, intracellular adhesion molecule, ALIX, CD81, CD63, epithelial cell adhesion molecule, annexin A5, and tumor susceptibility gene 101, using Exo-Check according to manufacturer's instructions (System Biosciences). Cis-golgi matrix protein 130 was used as a control for cellular contamination. In brief, a 300-μg exosome sample was lysed in radioimmunoprecipitation assay (RIPA) and incubated overnight on the array. Arrays were then incubated in detection buffer for 2 h at room temperature and imaged using SuperSignal West Femto Chemiluminescent Substrate (Thermo Fisher).

Proteomics and RNAseq on exosome samples. RNA sequencing was run at Genewiz using standard RNA-seq services Illumina HiSeq 2 × 150 bp analysis (Morrisville, NC). Data analysis was done using Ingenuity Pathway Analysis (IPA) software described below. Proteomics was conducted by Bioproximity using global proteomic profiling ultra-performance liquid chromatography tandem accurate mass spectrometry and up to 10,000 sequencing events (15-cm column, 20-min gradient; Chantilly, VA). Protein (Fig. 1*D*) acronyms are defined as follows: GPI, glucose-6-phosphate isomerase; ALDO, aldolase; TPI, triosephosphate isomerase; GAPDH, glyceraldehyde 3-phophate dehydrogenase; ENO, enolase; PGAM, phosphoglycerate mutase; PK, pyruvate kinase; OGDH, oxoglutarate dehydrogenase; ETFA, electron-transfer-flavoprotein-α; and ATPase, adenosine triphosphate synthase. Gene (Fig. 1*D*) acronyms are defined as follows: ALDOA, aldolase fructose-bysphosphate A; ENO3, enolase 3; GPI, glucose-6-phosphate isomerase; HK2, hexokinase 2; HK3, hexokinase 3; PFK, phosphofructokinase 1; PGM, pohsphoglucomutase 1; PK, pyruvate kinase; MDH2, malate dehydrogenase 2; OGDH, oxogluterate dehydrogenase; PC, pyruvate carboxylase; PDHA1, pyruvate dehydrogenase E1 α_1-subunit; PDHB, pyruvate dehydrogenase E1 β-subunit; SDHA, succinate dehydrogenase complex flavoprotein subunit A; SDHC, succinate dehydrogenase complex subunit C; SUCLG2, succinate-CoA ligase GDP-forming β-subunit; NDUFC2, NADH ubiquinone oxidoreductase subunit C2; NDUFB1, NADH ubiquinone oxidoreductase subunit B1; NDUFS5, NADH ubiquinone oxidoreductase subunit S5; NDUFA8, NADH ubiquinone oxidoreductase subunit A8; NDUFA9, NADH ubiquinone oxidoreductase subunit A9; NDUFS2, NADH ubiquinone oxidoreductase subunit S2; UQCRH1, ubiquinol-cytochrome-*c* reductase hinge 1; COX6c1, cytochrome-*c* oxidase subunit Vic; and COX10, heme A farnesyltransferase cytochrome-*c* oxidase assembly factor.

In vitro chronic hypoxia PASMC culture. Primary human PASMCs (Lonza) were cultured in DMEM with 10% FBS (Thermo Fisher) under standard culture conditions. At confluence, cells were rinsed with PBS and incubated in DMEM + 2% exosome-depleted FBS (SBI) with 10% well volume of PBS or exosome (EXSM) treatment at 4% oxygen (i.e., 200 μl of EXSM + 1.8 ml of PASMC culture media per well, in a 6-well plate format; ~2 × 10^7 exosomes per treatment). Cells were maintained in hypoxia for 2 wk, treated biweekly on culture *days 1*, *4*, *8*, and *11*. In EXSM dose response studies, PASMCs were treated biweekly with 1.25, 2.5, 5, and 10% well volume PBS or EXSM during hypoxic exposure (n = 4–8 per group for all PASMC studies). Cells and media were collected and frozen at −80°C for the assays described below. PASMC supernatant was collected (n = 8 per group), and citrate content was measured using a Citrate Assay Kit (Abcam, cat. no. ab83396), according to manufacturer's instructions. All PASMCs were used between passages 1 and 3 and were purchased commercially from Lonza as primary cells. Four different PASMC donors were used throughout

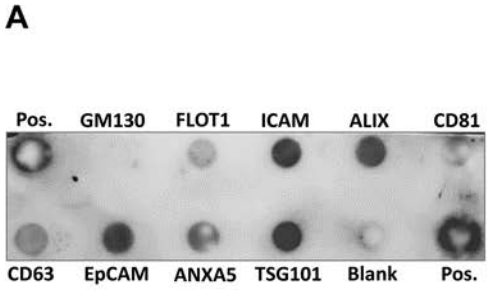

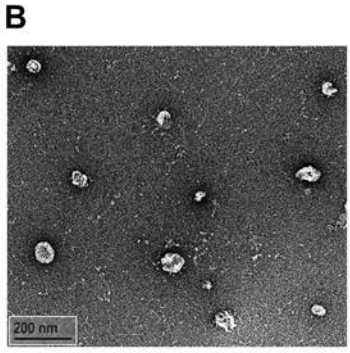

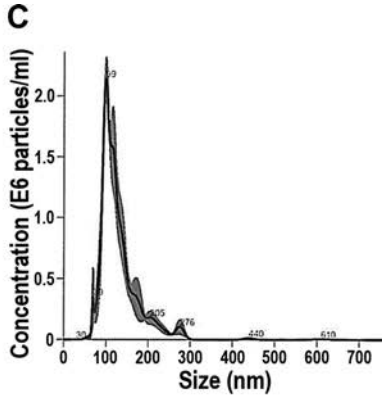

D

Pathway	Proteins	Genes
Glycolysis	GPI, ALDO, TPI, GAPDH, ENO, PGAM, PK	ALDOA, ENO3, GPI, HK2, HK3, PFK, PGM, PK
TCA Cycle	OGDH	MDH2, OGDH, PC, PDHA1, PDHB, SDHA, SDHC, SUCLG2
Electron Transport Chain	ETFA, ATPase	Complex I (NDUFC2, NDUFB1, NDUFS5, NDUFA8, NDUFA9, NDUFS2); Complex II (SDHA, SDHC); Complex III (UQCRH1); Complex IV (COX6c1, COX10); Complex V (39 ATPase genes enriched)

Fig. 1. Isolated exosomes demonstrate expression of known exosome markers and contain metabolic gene and protein content. *A*: Western blot array of exosome proteins. *B*: transmission electron microscopy imaging for exosome size and morphology. *C*: nanoparticle tracking for exosome size and concentration. *D*: proteomic and RNAseq analysis demonstrated that exosomes contain several proteins and genes involved in glycolysis, TCA cycle, and electron transport chain.

these studies (donor 1: male, Caucasian, 51 yr; donor 2: male, Hispanic, 35 yr; donor 3: female, African American, 34 yr; donor 4: female, Caucasian, 56 yr).

Metabolomics and microarray analysis. PASMCs were cultured and treated with EXSM or PBS after normoxia or chronic hypoxia exposure as described above ($n = 3$ for normoxia group, $n = 4$ for hypoxia and hypoxia + EXSM groups). PASMCs were pelleted, supernatant was aliquoted, and rat PAs were ground in liquid nitrogen. PAMSC pellets, supernatant aliquots, and rat PA were processed at Qiagen using illumine microarray HumanHT-12 v4 Expression Beadchip Array for microarray gene analysis. Cell pellets and conditioned media were processed at Metabolon using the global metabolomics platform which utilizes ultra-high-performance liquid chromatography/tandem accurate mass spectrometry and an in-house mLIMS metabolite standard library for metabolomics profiling. Metabolomics data was analyzed using Metabolync software (Metabolon, Morrisville, NC). Metabolite figure acronyms are defined as follows: Gly, glycine; Ser, serine; Thr, threonine; Ala, alanine; Asp, aspartate; Glu, glutamic acid; His, histidine; Lys, lysine; Phe, phenylalanine; Tyr, tyrosine; Trp, tryptophan; Leu, leucine; Ile, isoleucine; Val, valine; Met, methionine; Cys, cysteine; Tau, taurine; Arg, arginine; Pro, proline; Cre, creatine; PA, polyamine; GSH, glutathione; and GAA, γ-glutamyl amino acid.

IPA analysis. Gene expression fold changes between treatment and control groups were analyzed through the use of IPA (QIAGEN, https://www.qiagenbioinformatics.com/products/ingenuity-pathway-analysis). Briefly, an IPA core analysis using the HumanHT-12 v 4.0 reference set was performed to interpret data in the context of known (canonical) pathways and biological processes. Genes that were expressed below a log-2 fold change of 0.25 were removed from the analysis. To assess differential expression of specific targets [e.g., SIRT4, glutamate dehydrogenase 1 (GLUD1)] between treatment and control groups, custom pathways were created, and connections to canonical pathways were made through use of the IPA knowledgebase.

PASMC proliferation in vitro assay. PASMC proliferation was measured using the BrdU Cell Proliferation Assay Kit (Cell Signaling Technology, cat. no. 6813) and the Proliferating Cell Nuclear Antigen (PCNA) ELISA Kit (Cell Biolabs, cat. no. CBA-254). PASMCs (ATCC) were seeded at 2,000 cells/well in 96-well plates in DMEM with 10% FBS (Corning) under standard culture conditions for 24 h. PASMCs were rinsed with PBS and incubated in DMEM with 0.1% FBS to induce starvation conditions for 48 h. Cells were then treated with 0.5, 1, 3, 10, or 20% well volume of EXSM treatment or PBS ($n = 3$ per treatment), and FBS was added to 5% per well. Cells were incubated in normoxia or 4% oxygen for 4 days. In one plate, BrdU solution was added to wells and incubated for an additional 24 h in normoxia or 4% oxygen before fixing cells. Detection antibody and horseradish peroxidase-conjugated secondary antibody were added and the absorbance measured. Media was removed from another set of plates, and the cells were frozen at −80°C for 4 h. Cell lysate was extracted in RIPA Lysis Buffer (Thermo) overnight. Samples and standard were plated on an anti-PCNA-coated plate and stained with anti-PCNA and secondary horseradish peroxidase conjugate antibody. Absorbance of both BrdU and PCNA plates was measured at 450 nm.

Western blot analysis. PASMC lysates were prepared using RIPA buffer (Thermo Fisher). Bolt LDS sample buffer and Bolt reducing reagent (both from Thermo Fisher) were added to each lysate and incubated at 70°C for 10 min ($n = 4–8$ per group). Approximately 20 mg of flash-frozen rat gastrocnemius muscle was enriched for mitochondria using the cytochrome-*c* releasing apoptosis assay according to manufacturer instructions (Abcam, cat. no. ab65311). Tissue was processed on ice using kit-provided mitochondrial lysis buffers and a Tissue-Tearor 985370 (BioSpec Products, $n = 3$ per group). Lysates were separated on 10 or 12% Bolt Bis-Tris Plus Gels (Thermo Fisher) and transferred to nitrocellulose membranes using iBlot 2 Gel Transfer Device (Thermo Fisher). Membranes were probed with primary antibodies rabbit monoclonal GLUD1 (1:1,000; cat. no. ab168352), mouse monoclonal PDH cocktail (6 μg/ml, cat, no, ab110416), rabbit polyclonal pyruvate dehydrogenase kinase 4 (PDK4) (1:50, cat. no. ab71240), mouse monoclonal Actin (1:1,000; cat. no. ab3280), and mouse monoclonal β-actin (1:2,000; cat. no. ab8226; all antibodies from Abcam). Blot images were analyzed for band absorbance over background using GeneTools software (Syngene). Inclusion of a replicate control sample on multiple blots allowed for normalization of all samples to control.

RNA analysis. Total RNA was isolated using the RNeasy Mini Kit (Qiagen), and cDNA was made using the High-Capacity cDNA Reverse Transcription Kit (Thermo Fisher), according to manufacturer instructions ($n = 4$ per group). Taqman probes for SIRT4 (Hs01015516_g1) and peptidylprolyl isomerase A (Hs04194521_s1) were assessed using a QuantStudio 6 Flex Real-Time PCR System (all from Thermo Fisher).

PASMC oxygen consumption rate in vitro. A Seahorse XFp Analyzer (Agilent) was used to measure oxygen consumption rate (OCR). PASMCs were seeded in XFp miniplates, treated with 5, 15, or 30% well volume of PBS or EXSM, and exposed to hypoxia (4% oxygen) for 24 h ($n = 3$ per group). The Cell MitoStress Test Assay was performed according to manufacturer instructions. In brief, after the three initial baseline OCR measurements, oligomycin (1 μM) was injected into all samples to inhibit ATP synthase (thereby blocking state 3 respiration). The remaining OCR is assumed proton leak. To determine the maximal OCR that cells can sustain, the proton ionophore (uncoupler) carbonyl cyanide-4-(trifluoromethoxy)phenylhydrazone (FCCP) (4 μM) was injected. Lastly, a mix of rotenone and antimycin A (0.5 μM) was injected to inhibit electron flux through Complex III. Remaining OCR is due to the formation of mitochondrial reactive oxygen species and nonmitochondrial sources (61). OCR values were normalized to total protein measurements per well using a BCA Assay kit (Thermo Fisher). All negative OCR values were reported as zero in analyzed data.

Mouse model of hypoxia-induced PAH. All in vivo experiments were approved by the Institutional Animal Care and Use Committee and were carried out by CorDynamics. On study *day 1*, randomized naïve male C57BL/6 mice were administered a single intravenous dose of EXSM or PBS (lateral tail vein injection, 200 μl, ~2×10^7 particles per treatment) before hypoxic exposure. On study *day 2*, normoxic mice ($n = 7$) were maintained in ambient conditions, whereas hypoxic mice ($n = 8$) were maintained in 10% oxygen for 21 days. All animals were allowed food and tap water ad libitum. On terminal *day 22*, mice were euthanized, and a Millar pressure catheter was introduced through the right jugular vein to measure right ventricular systolic pressure (RVSP). The heart was removed, and the right ventricle (RV) and left ventricle with septum (LV+S) were weighed separately. Studies were performed and unbiased data compiled by CorDynamics.

Rat model of semaxanib/hypoxia-induced PAH. All in vivo experiments approved by the Institutional Animal Care and Use Committee and were carried out by CorDynamics as previously described (59). In brief, randomized adult (200–300 g) male Sprague-Dawley rats (65 total; $n = 5$ for normoxia control group, $n = 10$ for all other groups) were administered a single subcutaneous dose of semaxanib (20 mg/kg) on *day 1* of the study and maintained in chronic hypoxia (~13% oxygen) or normoxia for 28 days. All hypoxic groups were removed from hypoxia on *day 29* and placed in normoxic conditions for treatment until *day 56*. Control and treatment groups were dosed with a single intravenous EXSM or PBS injection every 3 days from *day 29* to *day 53* (200-μl exosome treatment, ~2×10^7 particles). Sildenafil treatment groups were administered an oral dose of Sildenafil (30 mg/kg) twice daily on *days 29–56*. All animals were allowed food and tap water ad libitum. On terminal *day 56*, rats were anesthetized by an intraperitoneal injection of ketamine-xylazine (80/10 mg/kg), and a fluid-filled pressure catheter was introduced into the right jugular vein to measure systolic PA pressure (SPAP). After

rats were euthanized, the heart was removed, infused with saline until clear, and ventricles were weighed separately (RV, RV/LV+S). PAs and gastrocnemius skeletal muscle were removed and frozen at −80°C for metabolomics and protein analysis, respectively. Studies were performed and unbiased data were compiled by CorDynamics.

Nanoparticle tracking analysis. Exosome particle analysis was outsourced to Particle Technology Group LLC nanoparticle tracking analysis services. Exosome concentration and size were measured using a Nanosight NS300 (Malvern), according to manufacturer instructions.

Transmission electron microscopy. Exosome transmission electron microscopy (TEM) imaging was outsourced to the University of North Carolina at Chapel Hill Microscopy Services Laboratory in the Pathology and Laboratory Medicine Department. Exosomes were prepared by negative staining with 2% sodium phosphotungstate, pH 7.0. Grids were floated on 15-μl droplets of exosome suspension and incubated for 20 min, transferred to a 25-μl droplet of 1% glutaraldehyde in 0.15 M sodium phosphate buffer, pH 7.4, and fixed for 5 min. After a brief rinse on 2 sequential droplets of deionized water, the grids were transferred to a 25-μl droplet of 2% sodium phosphotungstate and stained for 1 min. Samples were observed with a JEOL JEM-1230 transmission electron microscope operating at 80 kV (JEOL USA, Peabody, MA), and digital images were acquired using a Gatan Orius SC1000 CCD camera and Gatan Microscopy Suite 3.0 software (Gatan, Inc., Pleasanton, CA).

Statistical Analysis. All values are expressed as means ± SE and analyzed using an unpaired, two-tailed Student's *t*-test. All comparisons between experimental groups were performed using a one-way ANOVA with Tukey's multiple comparisons test using GraphPad PRISM 7.3 statistical software, unless otherwise indicated.

RESULTS

Bone marrow MSC-derived exosomes are enriched in metabolic proteins and genes. To characterize bone marrow MSC-derived exosomes, exosome protein, vesicle size, and metabolic protein and gene content were evaluated. Isolated exosomes expressed flotillin-1, intracellular adhesion molecule, ALIX, CD81, CD63, epithelial cell adhesion molecule, annexin A5, and tumor susceptibility gene 101 (exosome-specific proteins) and were devoid of Cis-golgi matrix protein 130, a Golgi apparatus protein (cellular contamination; Fig. 1*A*). TEM imaging and nanoparticle tracking analysis demonstrated that

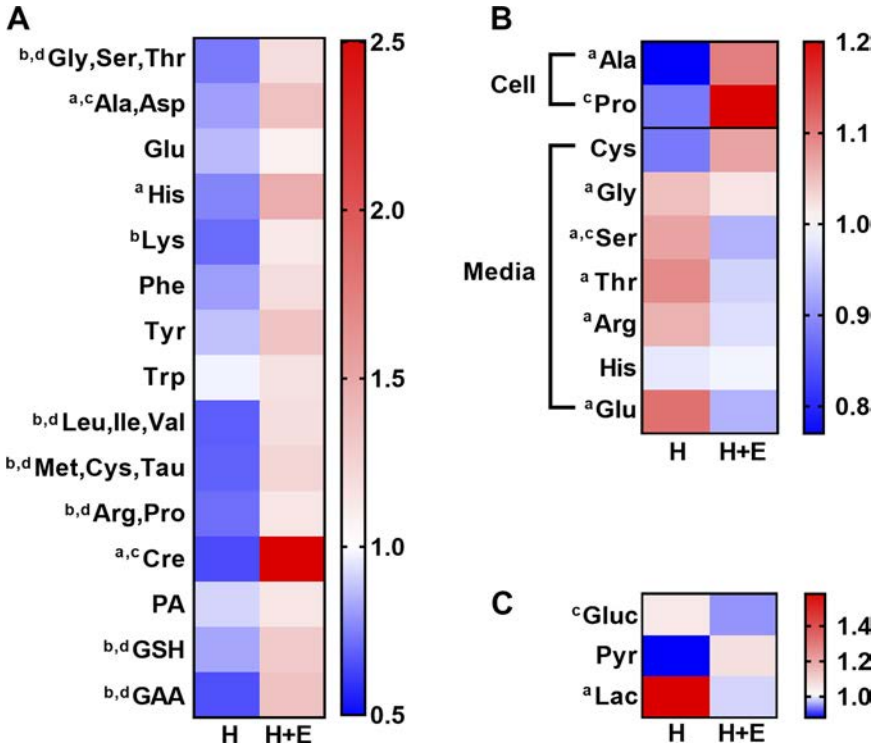

Fig. 2. Exosomes increase global amino acid (AA) metabolism and boost mitochondrial efficiency, oxygen consumption rate, and energetics in pulmonary artery smooth muscle cells (PASMCs) exposed to chronic hypoxia. PASMCs were cultured in normoxia or chronic hypoxia (4% oxygen for 2 wk), and metabolite analysis of cell lysates was performed. *A*: heat map analysis of AA metabolites. Data are represented as mean ± SE of AA in each group. *B*: heat map of amino acids present in cell culture supernatant after chronic hypoxia exposure. Amino acids were present in the cell growth media (media) or not (cell). *C*: heat map of glucose (Gluc), pyruvate (Pyr), and lactate (Lac) levels in PASMC culture supernatant after chronic hypoxia exposure. "H" denotes the fold change of hypoxia/normoxia, and "H+E" denotes the fold change of hypoxia + exosome treatment/hypoxia. $^{a}P < 0.05$ and $^{b}P < 0.01$ represent hypoxia compared with normoxia treatments, and $^{c}P < 0.05$ and $^{d}P < 0.01$ represent hypoxia + exosome treatment compared with hypoxia. *D*: average of TCA metabolites in PASMC culture supernatant. *E*: citrate alone in PASMC culture supernatant. *F*: oxygen consumption rate (OCR) in PASMCs after acute hypoxia exposure with increasing exosome treatment. Compounds oligomycin (1 μM), carbonyl cyanide-4-(trifluoromethoxy)phenylhydrazone (FCCP) (4 μM), and a mix of rotenone and antimycin A (0.5 μM) were serially injected into all samples and background wells to measure ATP production, maximal respiration, and nonmitochondrial respiration, respectively. *G*: creatine, phosphocreatine (PCr), nicotinamide, nicotinamide ribonucleotide (NMN), and adenosine in PASMC lysates. *H*: heatmap of genes associated with mitochondrial damage [heat shock protein 90 (HSP90), TNF, and FASLG] and mitochondrial health/homeostasis (COX4, LMX1B, and TP53) in PASMC lysates. *I*: PASMC proliferation after 4 days of normoxia or hypoxia exposure with increasing exosome treatment BrdU (*left*; light gray bars) or proliferating cell nuclear antigen (PCNA; *right*; dark gray bars). $\$P \leq 0.1$ compared with normoxia, $*P \leq 0.05$ and $**P \leq 0.01$ represent hypoxia compared with normoxia treatments, and $\#P \leq 0.05$ and $\#\#P \leq 0.01$ represent hypoxia + exosome treatment compared with hypoxia. COX4, cytochrome-*c* oxidase subunit 4; EXSM, exosome; LMX1B, LIM homeobox transcription factor-1β; TP53, tumor protein P53.

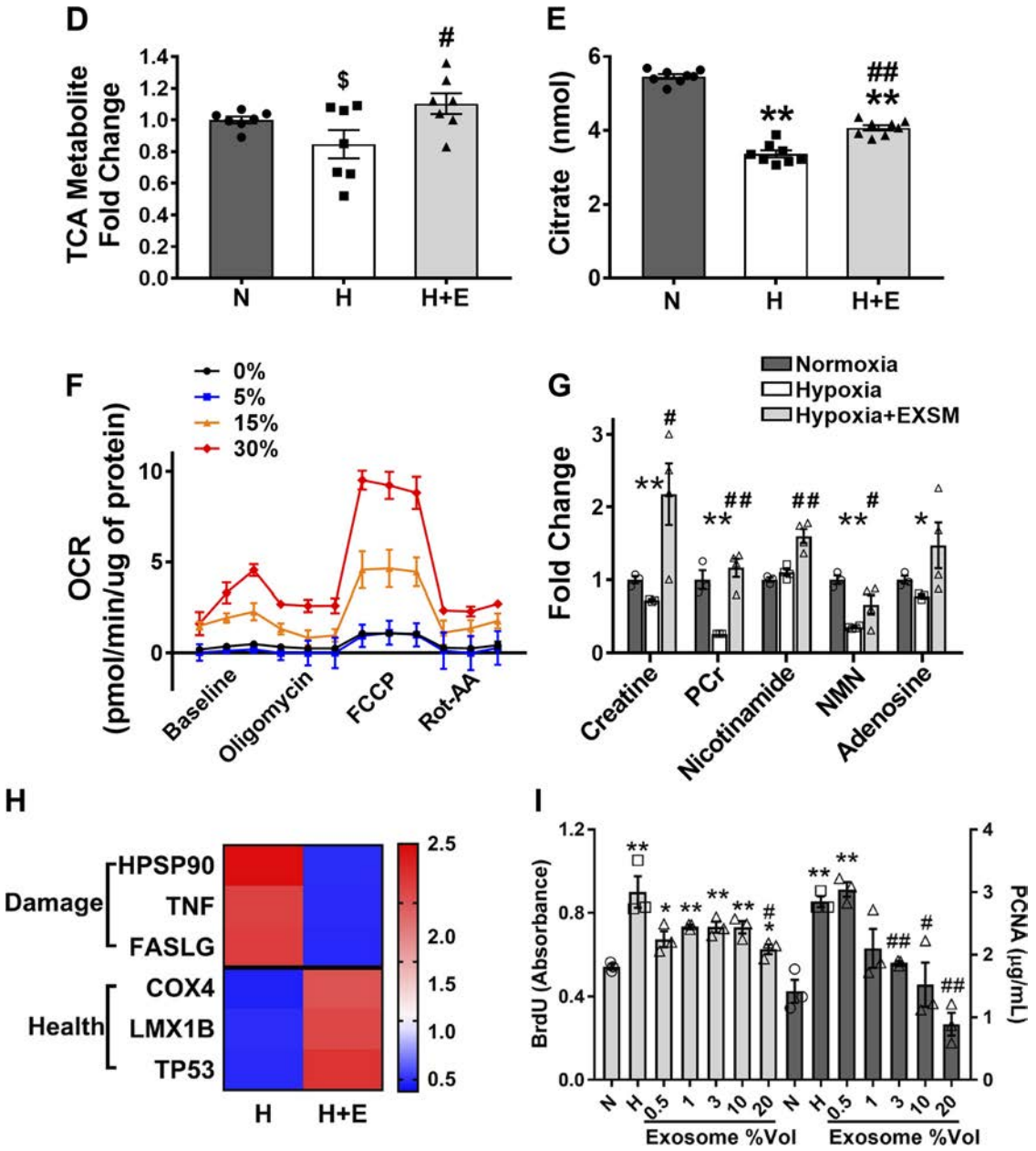

Fig. 2—*Continued*.

exosomes range between 50 and 150 nm in size and have an average concentration of 1×10^8 particles/ml (Fig. 1, *B* and *C*). Proteomics and RNA sequencing analysis revealed that exosomes are enriched with metabolic protein and gene content (Fig. 1*D*). These findings provided the impetus for the evaluation of exosomes in host cell mitochondrial function.

Exosomes improve amino acid metabolism in hypoxia. Metabolic dysfunction consistent with the Warburg effect contributes to the pathogenesis of PAH (13). PASMCs cultured in hypoxia are often used as an in vitro tool to study the metabolic changes associated with PAH (42). Thus, we conducted a global metabolite analysis of human PASMCs cultured in chronic hypoxia with exosome treatment to explore the effect of exosomes on metabolic dysfunction in PAH. These data revealed a decrease in amino acids (AAs) after hypoxia exposure compared with normoxia control (Fig. 2*A*, *left* column), demonstrating a decline in global AA metabolism. Inversely, exosome treatment increased AA levels compared with hypoxia alone (Fig. 2*A*, *right* column). These data are indicative of an exosome-mediated boost in AA metabolism during chronic hypoxia exposure.

We further assessed metabolite uptake and production via analysis of PASMC culture supernatant. Of the metabolites present in the supernatant, cysteine, glycine, serine, threonine, arginine, histidine, and glutamic acid were present in the cell culture growth media, whereas alanine and proline were not. Hypoxic supernatant contained less alanine and proline than normoxic supernatant, reflecting a decrease in production. Exosome treatment increased these metabolites compared with hypoxic supernatant alone (Fig. 2*B*, *top* heat map). Impor-

tantly, the opposite was found in metabolite uptake of PASMCs. AAs contained in the culture media were found in higher levels in hypoxic supernatant compared with normoxic supernatant, suggesting a decline in AA uptake or cellular production, likely because of their diminished metabolism. Exosome treatment decreased levels of these metabolites, indicative of increased metabolite consumption compared with hypoxia alone (Fig. 2*B*, *bottom* heat map). These data demonstrate that chronic hypoxia suppresses both uptake and production of AAs, whereas exosome pretreatment reinstates AA metabolism.

Exosomes increase glucose oxidation and prevent a shift to glycolysis and mitochondrial damage in chronically hypoxic PASMCs. A dysfunction in AA consumption could suggest a decrease in oxidative metabolism and thus a metabolic shift toward glycolysis. In support of this hypothesis, PASMCs are known to undergo a glycolytic shift after hypoxia exposure and in animal models of PAH (3, 37). Herein, we show that lactate levels were dramatically increased in the hypoxic supernatant compared with normoxia, consistent with increased rates of glycolysis. Importantly, exosome treatment decreased lactate and glucose levels in the supernatant compared with hypoxia alone (Fig. 2*C*), reflecting increased glucose uptake and decreased lactate production. These data are highly suggestive of increased flux into oxidative metabolism.

To further understand the exosome effects on glucose oxidation, TCA cycle metabolites in PASMC supernatant were assessed. Although chronic hypoxia decreased TCA metabolites, exosome pretreatment normalized these levels (Fig. 2*D*). The first metabolite within the TCA cycle, citrate, followed the same trend when measured independently. Citrate levels were decreased after hypoxic exposure and normalized with exosome treatment (Fig. 2*E*). These data demonstrate a decrease in TCA cycle metabolites after hypoxia exposure, an effect that was mitigated with exosome treatment.

To determine the functional impact of exosome treatment on oxidative phosphorylation, OCR was measured in PASMCs after acute (24-h) hypoxia exposure. Exosome pretreatment dramatically increased OCR of hypoxic PASMCs in a dose-dependent manner, increasing OCR up to 15-fold over hypoxia control with exosome treatment (Fig. 2*F*). These data directly demonstrate a beneficial effect of exosomes on mitochondrial function in hypoxia. Because increased oxygen consumption is suggestive of increased energy production in the cell, we assessed various building blocks of energy sources—namely creatine, phosphocreatine, nicotinamide, nicotinamide ribonucleotide, and adenosine. Acute hypoxia exposure decreased creatine, phosphocreatine, and nicotinamide ribonucleotide compared with normoxia, whereas exosome treatment increased these metabolites compared with hypoxia alone (Fig. 2*G*). The hypoxia-induced decrease in these energy precursors suggests a decrease in energy production through the creatine, NAD, and ATP pathways, which was curbed with exosome treatment. These data demonstrate that hypoxia exposure decreased oxygen consumption (data not shown) and energy production in PASMCs, both of which were prevented by exosome treatment.

Because decreased TCA cycle metabolism and oxygen consumption are indicative of mitochondrial dysfunction, PASMCs were evaluated for genes associated with mitochondrial damage. Hypoxia exposure increased levels of heat shock protein 90, tumor necrosis factor-α, and fas ligand tumor necrosis factor superfamily member 6, reflective of the mitochondrial damage seen in PAH (10, 18, 36, 63). Inversely, cytochrome-*c* oxidase subunit 4, LIM homeobox transcription factor-1β, and tumor protein P53, indicators of healthy mitochondrial function, were decreased after hypoxia exposure, similar to PAH

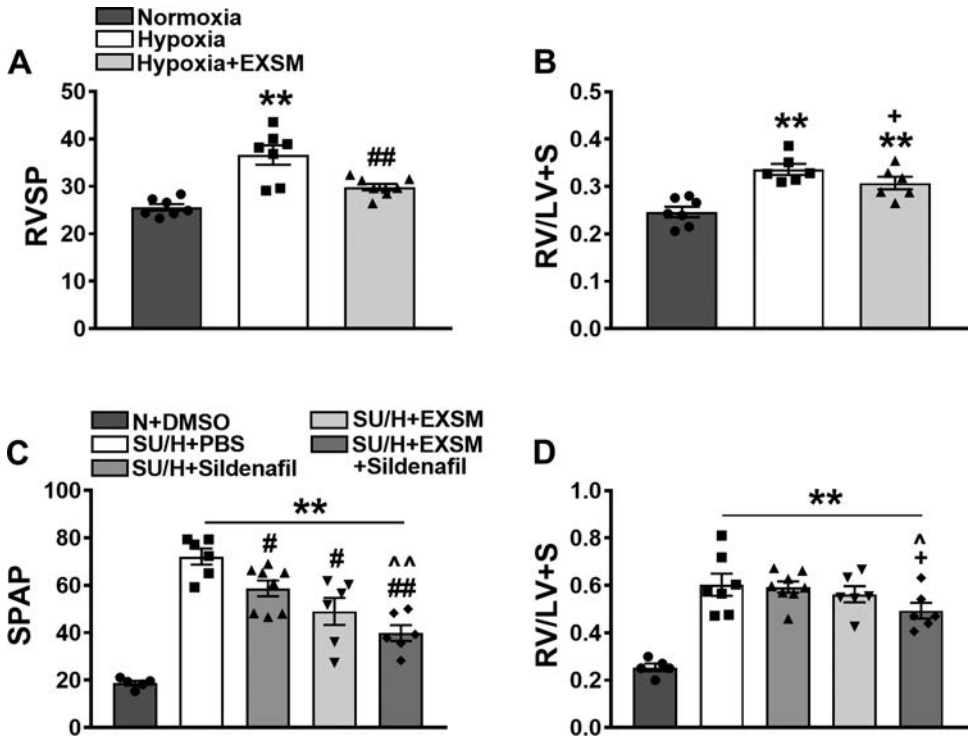

Fig. 3. Exosome therapy improves pulmonary arterial hypertension (PAH) pathogenesis in mouse and rat models of disease. Right ventricular systolic pressure (RVSP) (*A*) and right ventricle/left ventricle and septum (RV/LV+S; Fulton index) (*B*) were measured in a hypoxia-induced mouse model of PAH. Systolic pulmonary artery pressure (SPAP) (*C*) and RV/LV+S (*D*) were measured in a semaxanib/hypoxia rat model of PAH with Sildenafil background therapy. $^{**}P \leq 0.01$ compared with normoxia and N+DMSO; $+P \leq 0.1$, $\#P \leq 0.05$, and $\#\#P \leq 0.01$ compared with hypoxia and SU/H+PBS; and $\wedge P \leq 0.05$ and $\wedge\wedge P \leq 0.01$ compared with SU/H + Sildenafil. N + DMSO, normoxia + dimethyl sulfoxide; SU/H + EXSM, semaxanib/hypoxia + exosome treatment; SU/H + EXSM + Sildenafil, semaxanib/hypoxia + exosome treatment + Sildenafil; SU/H + PBS, semaxanib/hypoxia + PBS; SU/H + Sildenafil, semaxanib/hypoxia + Sildenafil.

pathogenesis (15, 26, 34). Importantly, this gene expression profile was reversed by exosome treatment, suggesting that exosomes prevent the mitochondrial damage associated with chronic hypoxia (Fig. 2*H*, *right*). Lastly, PASMC hyperproliferation is a trademark characteristic of PAH pathogenesis and decreased mitochondrial function (50, 52). Thus, we assessed PASMC hyperproliferation in hypoxia after exosome exposure. Although hypoxic exposure increased PCNA and BrdU measures of PASMC proliferation, exosome treatment decreased proliferation in a dose-responsive manner (Fig. 2*I*).

Exosome treatment improves PAH pathogenesis in a mouse and rat model. We next sought to evaluate the translational relevance of these findings in two rodent models of PAH. The first model evaluated mice after chronic hypoxia exposure. Hypoxic stress yielded increased RVSP and RV/LV+S weight ratio (Fulton index), reflective of decreased vascular remodeling in PAH (39, 52). Exosome pretreatment partially reversed the hypoxia-mediated elevation in RVSP and decreased Fulton index compared with disease control ($P < 0.1$; Fig. 3, *A* and *B*).

Similarly, treatment benefits were observed in a second, more severe rodent model of PAH. Exposure of rats to semaxanib/hypoxia (SU/H) resulted in increased SPAP and Fulton index compared with control rats. Sildenafil, a commercially available treatment for PAH, is often used as a clinically relevant background therapy in models of PAH (6). Thus, to demonstrate a benefit over standard-of-care therapy (9), exosome treatment was tested alone and in combination with Sildenafil. Sildenafil and exosomes both decreased SPAP compared with disease control. However, the combination therapy had an additive effect, reducing SPAP by almost 2-fold (Fig. 3*C*). In agreement with previous studies, Sildenafil alone did not affect the Fulton index, likely reflective of the robust nature of the SU/H PAH model (6). Although exosome treatment trended to decrease the Fulton index, the combination therapy significantly reduced RV/LV+S compared with disease control (Fig. 3*D*). Although these data suggest an exosome-mediated improvement in vascular remodeling, cardiac output was not measured, and thus we cannot rule out the possible contribution of impaired RV function to treatment benefits. In aggregate, these data support the claim that exosome treatment can both prevent and reverse PAH pathogenesis (2, 31).

Exosome treatment increases mitochondrial metabolism in a rat model of PAH. Because derangements in mitochondrial function are known to exist in PAH, we sought to investi-

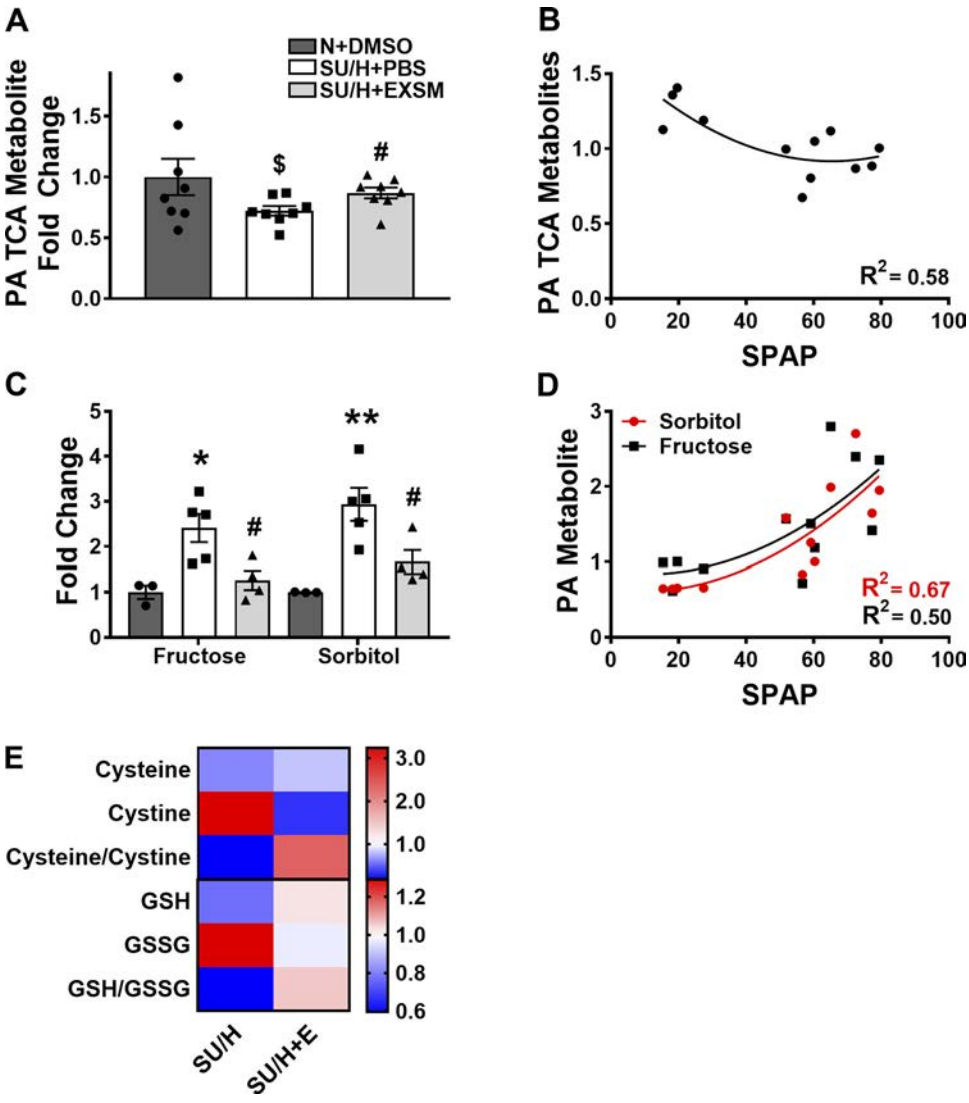

Fig. 4. Exosome therapy ameliorates glucose oxidation, reactive oxygen species, and mitochondrial damage in a semaxanib/hypoxia rat model of pulmonary arterial hypertension (PAH). Average of TCA cycle metabolites (*A*), fructose and sorbitol (*C*), and cysteine/cysteine ratio and glutathione (GSH)/glutathione disulfide (GSSG) ratio (*E*) in the pulmonary artery (PA) of rats. Systolic pulmonary artery pressure (SPAP) correlated to PA (*B*) TCA cycle metabolites and (*D*) fructose and sorbitol. SU/H denotes the fold change of control/PAH and SU/H + E denotes the fold change of exosome-treated PAH/PAH. Control (N + DMSO), PAH (SU/H + PBS), and PAH after exosome treatment (SU/H + EXSM). $\$P \leq 0.1$ compared with N + DMSO, $^*P \leq 0.05$ and $^{**}P \leq 0.01$ compared with N + DMSO, and $\#P \leq 0.05$ compared with SU/H + PBS. N + DMSO, normoxia + dimethyl sulfoxide; SU/H + EXSM, semaxanib/hypoxia + exosome treatment; SU/H + PBS, semaxanib/hypoxia + PBS.

gate the potential impact of exosome therapy on PAH-induced metabolic dysfunction. Metabolomics analysis of rat PAs revealed decreased levels of TCA cycle metabolites in disease compared with control, whereas exosome treatment demonstrated an increase in these metabolites (Fig. 4*A*). Correlation analysis of SPAP and TCA cycle metabolites demonstrated a negative correlation, indicating that rats with improved SPAP had elevated TCA cycle intermediates (Fig. 4*B*). These data mirror PASMC metabolomics data (Fig. 2), demonstrating that exosome treatment increased flux through the TCA cycle, both in vitro and in vivo.

Decreased TCA cycle function and subsequent dependence on glycolysis are known to result in the accumulation of fructose and sorbitol in PAH (67). Metabolomics data indicated a greater than twofold increase in fructose and sorbitol levels in the PA of disease rats compared with control, which was normalized with exosome treatment (Fig. 4*C*). Furthermore, a positive correlation was seen between SPAP and both fructose and sorbitol, demonstrating that rats with improved SPAP had diminished levels of fructose and sorbitol (Fig. 4*D*). These findings complement PASMC in vitro data demonstrating that exosome treatment increases glucose flux through glucose oxidation and away from glycolysis (Fig. 2).Additionally, redox couples such as GSH/reduced glutathione and cysteine/cystine are widely used as indicators of mitochondrial and extracellular oxidative stress in various disease models (68). Herein, GSH/ reduced glutathione and cysteine/cystine ratios were decreased in PAH compared with control, whereas exosome treatment increased both ratios after hypoxia exposure (Fig. 4*E*). These data suggest that exosome treatment decreased oxidative stress in PAH.

Exosomes upregulate PDH and GLUD1 in hypoxia. To identify the mechanism by which exosomes improve TCA cycle metabolism in hypoxia and PAH, PASMC AAs were mapped to their appropriate entry points into the TCA cycle. These data revealed a pattern wherein exosome treatment impacted specific entry points, namely the pyruvate and glutamine pathways. Hypoxic exposure decreased AAs entering the TCA cycle through all entry points (acetyl-CoA, a-ketoglutarate, succinyl-CoA, fumarate, and oxaloacetate compared with normoxia) (Fig. 5, *left* bars). Exosome treatment increased AAs entering the TCA cycle through acetyl-CoA via PDH and a-ketoglutarate through GLUD1 only (Fig. 5, *right* bars), demonstrating that exosome treatment increased flux into the TCA cycle through targeting these pathways.

To further explore exosome therapeutic targeting of PDH and GLUD1, microarray gene expression analysis of PASMCs in chronic hypoxia was performed. Both PDH and GLUD1 mRNA, known to be inhibited by hypoxia-inducible factor 1-α (HIF1-α) signaling in hypoxia, are reduced in PAH (55, 56). In

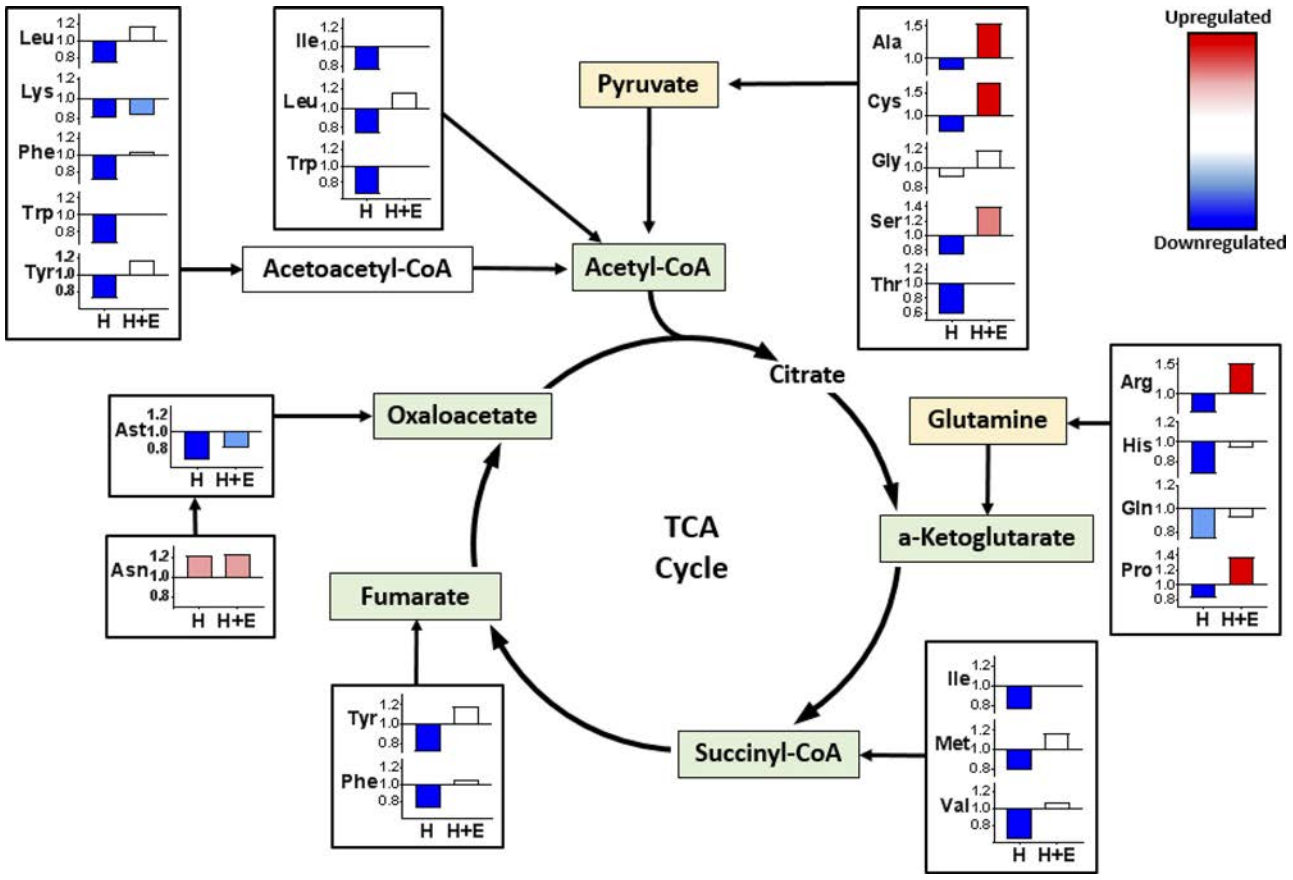

Fig. 5. Exosome pretreatment increases amino acid metabolites in pulmonary artery smooth muscle cells (PASMCs) after chronic hypoxia exposure through pyruvate dehydrogenase and glutamate dehydrogenase 1 entry points of the TCA cycle. PASMCs were cultured in normoxia or chronic hypoxia (4% oxygen for 2 wk), and metabolite analysis of cell lysates was performed. TCA cycle metabolite levels are shown. H denotes the fold change of hypoxia/normoxia, and H+E denotes the fold change of hypoxia + exosome treatment/hypoxia. Dark blue: $P \leq 0.05$ downregulation of hypoxia compared with normoxia. Red: $P \leq 0.05$ upregulation of hypoxia + exosome treatment compared with hypoxia.

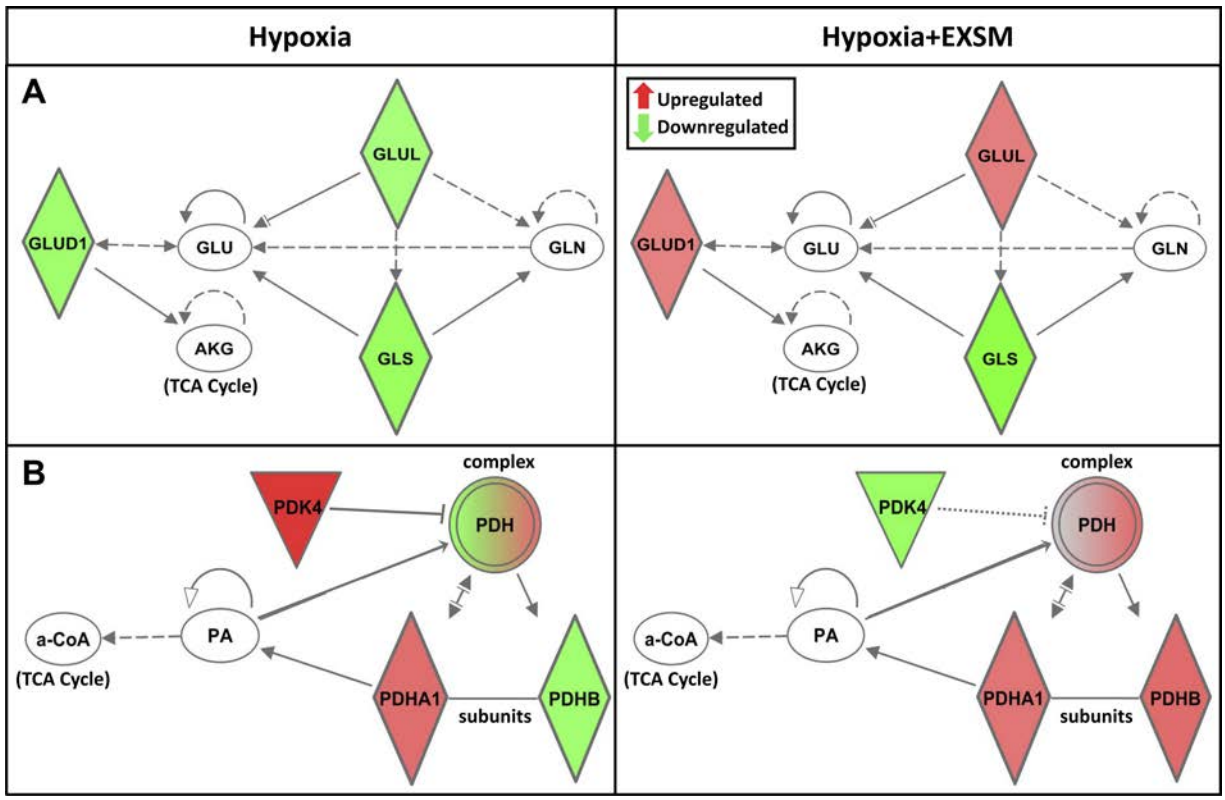

Fig. 6. Exosome pretreatment upregulates pyruvate dehydrogenase (PDH) and glutamate dehydrogenase 1 (GLUD1) gene expression in pulmonary artery smooth muscle cells (PASMCs) after chronic hypoxia. PASMCs cultured in normoxia or chronic hypoxia (4% oxygen for 2 wk) were analyzed via microarray analysis. GLUD1 (*A*) and PDH (*B*) pathway gene expression was assessed. The *left* represents the hypoxia/normoxia fold change, whereas the *right* represents the hypoxia + exosome treatment/hypoxia fold change. Red denotes upregulation, and green denotes downregulation of gene expression. a-CoA, acetyl-coenzyme A; AKG, 2-oxoglutaric acid, GLN, glutamine; GLS, glutaminase; GLU, L-glutamic acid; GLUL, glutamine synthetase; PA, pyruvic acid; PDHA1, pyruvate dehydrogenase subunit-α_1; PDHB, pyruvate dehydrogenase subunit-β; PDK4, pyruvate dehydrogenase kinase 4.

support of these previous reports, microarray analysis indicated that PDH and GLUD1 were downregulated in hypoxia compared with normoxia (Fig. 6, *A* and *B*, *left*), a phenotype which was prevented with exosome treatment (Fig. 6, *A* and *B*, *right*). Furthermore, PDK4, an inhibitor of PDH which is upregulated in patients with PAH, was elevated in hypoxia (65). This increase in gene expression was prevented by exosome treatment (Fig. 6*B*). Consistent with the metabolite data, these gene expression trends imply decreased flux into the TCA cycle after hypoxic exposure. Exosomes prevented this through upregulation of the PDH and GLUD1 pathways.

Since exosome treatment upregulates both PDH and GLUD1 gene expression in hypoxia, we next sought to determine if protein levels were likewise regulated. To this end, PDH, GLUD1, and PDK4 protein expression was assessed in hypoxic PASMCs. Hypoxic exposure decreased PDH and GLUD1 but increased PDK4 protein expression compared with normoxia, whereas exosome treatment prevented these changes, maintaining high levels of PDH and GLUD1 and low levels of PDK4 protein (Fig. 7, *A–C*). Furthermore, increasing doses of exosome treatment resulted in a dose-responsive increase in PDH and GLUD1 and a decrease in PDK4 protein expression (Fig. 7, *D–F*). In complex, these data demonstrate exosome upregulation of PDH and GLUD1 pathways at both the gene and protein levels in prolonged hypoxia.

The SIRT4 hypothesis: exosome treatment targets upstream regulator of PDH and GLUD1. SIRT4 has been shown to inhibit both PDH and GLUD1 activity and metabolism through separate processes, though little is known about its activity in hypoxia (21, 38). We hypothesized that (*1*) hypoxic exposure activates SIRT4 to serve as an energy-sparing safeguard in response to hypoxic stress, and (*2*) exosome treatment inhibits SIRT4, removing the blockage and upregulating both PDH and GLUD1 pathways. In support of this hypothesis, microarray gene expression revealed SIRT4 to be upregulated after chronic hypoxia and downregulated with exosome treatment compared with hypoxia control (Fig. 8*A*). These data suggest a hypoxia-induced upregulation of SIRT4, which could inhibit GLUD1 and PDH. Exosome treatment removes this SIRT4 blockage, restoring GLUD1 and PDH pathways.

Moreover, SIRT4 gene expression in PASMCs with increasing time in hypoxia was assessed. Quantitative RT-PCR showed that SIRT4 gene expression increased over time in hypoxia-exposed PASMCs compared with normoxic control. Exosome pretreatment downregulated SIRT4 gene expression after 7 and 14 days in hypoxia compared with hypoxic control alone (Fig. 8*B*). These data indicate that SIRT4 upregulation is driven by sustained hypoxic exposure, whereas exosome treatment prevents this change. Additionally, increasing doses of exosomes decreased SIRT4 gene expression (Fig. 8*C*), supporting the notion that exo-

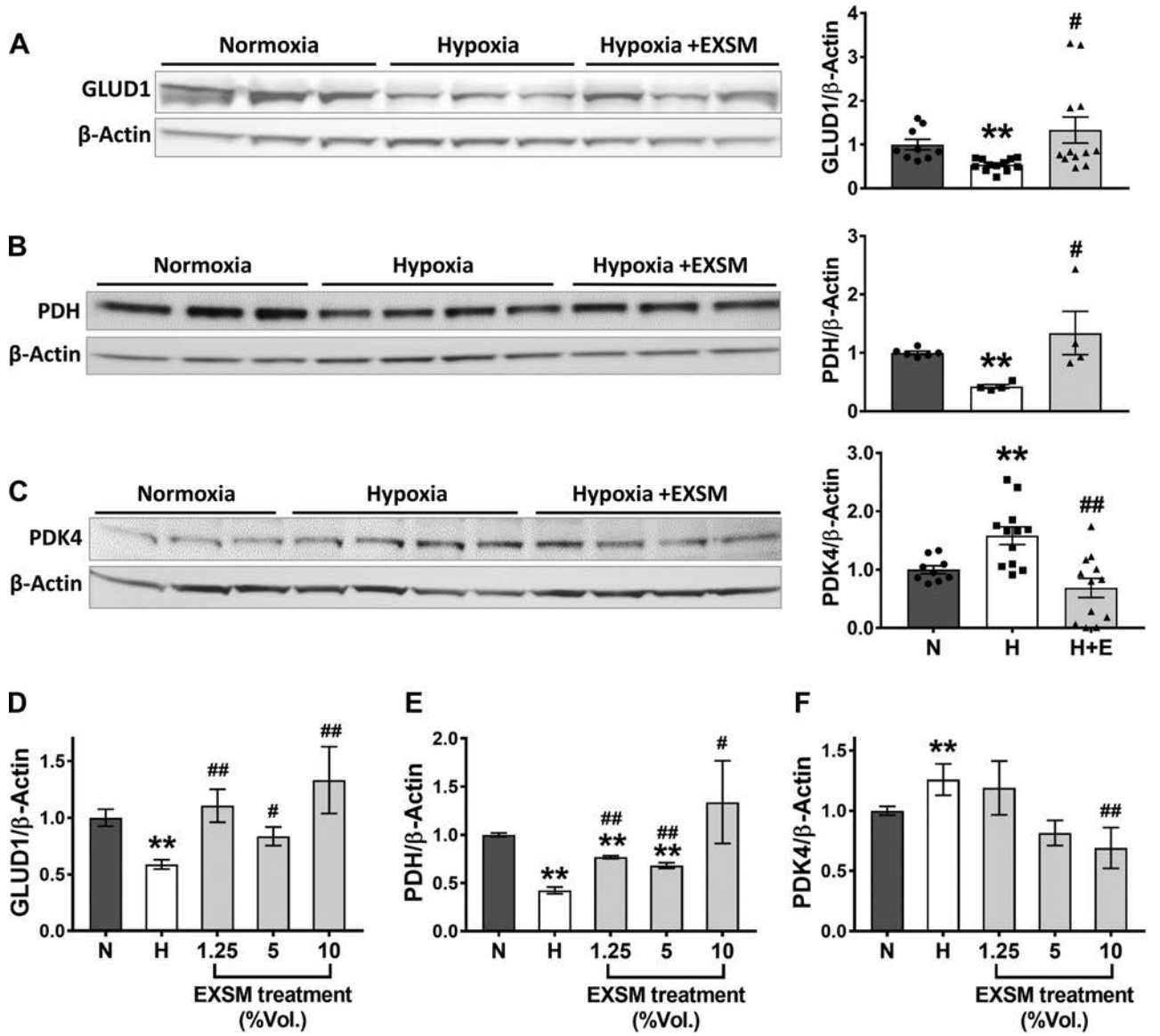

Fig. 7. Exosome pretreatment increases glutamate dehydrogenase 1 (GLUD1) and pyruvate dehydrogenase (PDH) but decreases pyruvate dehydrogenase kinase 4 (PDK4) protein expression in chronic hypoxia. Pulmonary artery smooth muscle cells (PASMCs) were cultured in normoxia or chronic hypoxia (4% oxygen for 2 wk) with and without exosome treatment (10% volume). GLUD1 (*A*), PDH (*B*), and PDK4 (*C*) protein expression. Three blots were included in analysis of GLUD1 and PDK4, and 2 blots were included in PDH analysis. PASMCs cultured in normoxia or chronic hypoxia with increasing exosome doses of 1.25, 5, and 10% volume are shown. GLUD1 (*D*), PDH (*E*), and PDK4 (*F*) protein expression, inclusive of data from *A*–*C*. $^{**}P \leq 0.01$ represent hypoxia compared with normoxia treatments, and $\#P \leq 0.05$ and $\#\#P \leq 0.01$ represent hypoxia + exosome treatment compared with hypoxia. H, hypoxia; H+E, hypoxia with exosome treatment; N, normoxia.

somes downregulate SIRT4 gene expression in hypoxia, even at low doses. These data support the hypothesis that SIRT4, upstream of PDH and GLUD1, may function to reduce nutrient flux into the mitochondria under conditions of hypoxic stress. Exosomes may function to release this block by inhibiting SIRT4 and reestablishing flux through the TCA cycle and mitochondrial metabolism.

Proposed role of exosomes in mitochondrial metabolism in PAH. The data herein support the idea that in hypoxic PASMCs, SIRT4 is activated as an energy-sparing safeguard to allow cells to survive under hypoxic stress. SIRT4, an upstream regulator of mitochondrial PDH and GLUD1, decreases pyruvate and glutamine entry into the TCA cycle by inhibiting these enzymatic entry points. Decreased PDH activity is further exacerbated by the activation of known inhibitor PDK4. This blockage results in an overall reduction of mitochondrial function (Fig. 9, *left*). Exosome treatment inhibits SIRT4 and PDK4, potentially removing the blockage on PDH and GLUD1 and restoring glutamine and pyruvate flux into the TCA cycle, thereby reestablishing mitochondrial function (Fig. 9, *right*).

DISCUSSION

The current study sought to examine the potential role of exosome therapy in PAH-associated mitochondrial dysfunc-

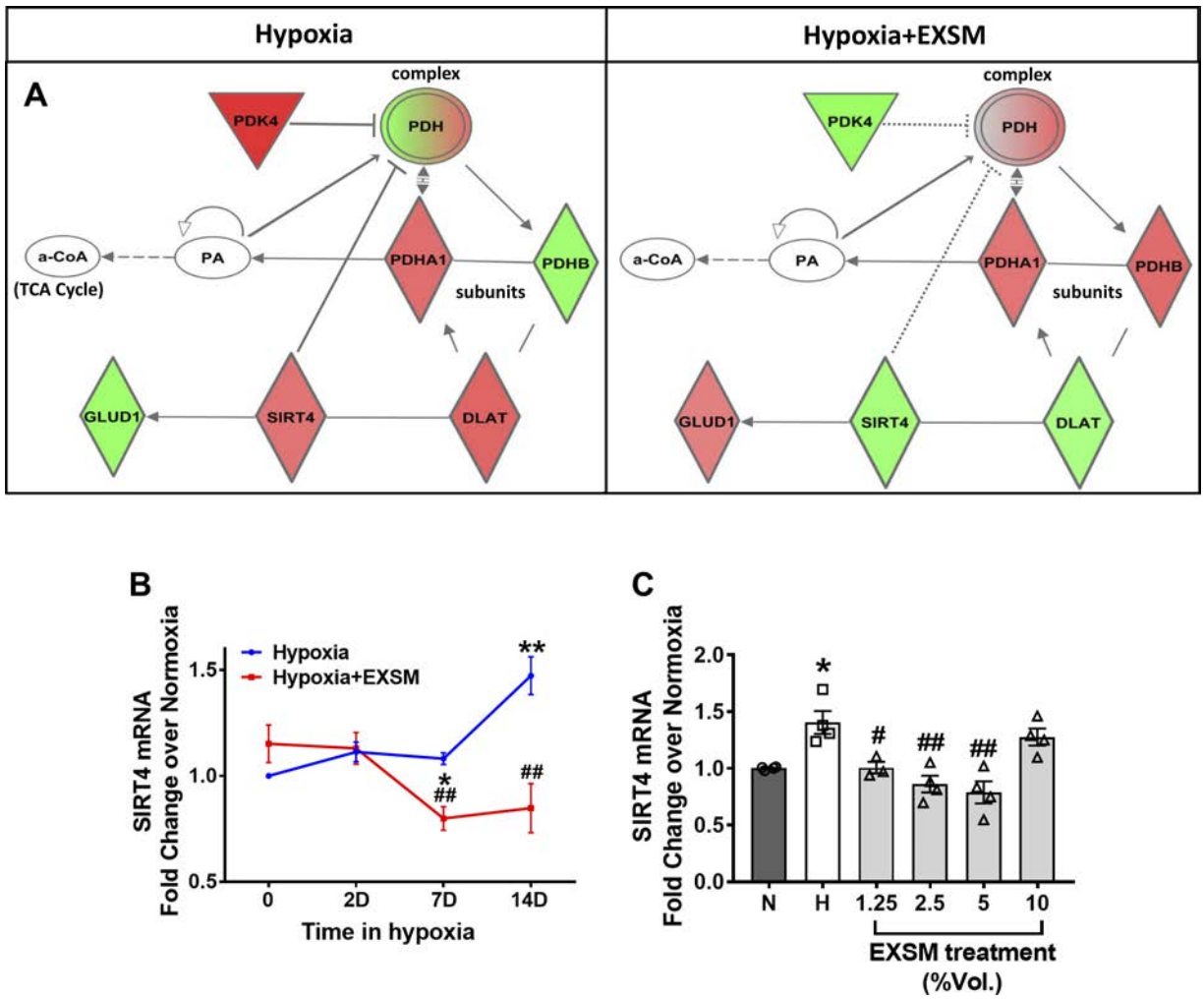

Fig. 8. Exosome treatment downregulates sirtuin 4 (SIRT4) gene expression of pulmonary artery smooth muscle cells (PASMCs) in chronic hypoxia. PASMCs were cultured in normoxia or chronic hypoxia (4% oxygen for 2 wk). *A*: global microarray analysis on the SIRT4 pathway was performed ($n = 4$ per group). The *left* represents the hypoxia/normoxia fold change, whereas the *right* represents the hypoxia + exosome treatment/hypoxia fold change. Red denotes upregulation, and green denotes downregulation. *B*: SIRT4 gene expression in PASMCs over time in hypoxia after exosome treatment (10% volume). "D" denotes days in hypoxia. *C*: SIRT4 gene expression after increasing doses of exosome treatments. $*P \leq 0.05$ and $**P \leq 0.01$ represent hypoxia compared with normoxia treatments, and $\#P \leq 0.05$ and $\#\#P \leq 0.01$ represent hypoxia + exosome treatment compared with hypoxia. a-CoA, acetyl-coenzyme A; DLAT, dihydrolipoamide acetyltransferase component of pyruvate dehydrogenase; EXSM, exosome; GLUD1, glutamate dehydrogenase; H, hypoxia; N, normoxia; PA, pyruvic acid; PDH, pyruvate dehydrogenase complex; PDHA1, pyruvate dehydrogenase subunit-α_1; PDHB, pyruvate dehydrogenase subunit-β; PDK4, pyruvate dehydrogenase kinase 4.

tion. Although a glycolytic shift occurs in PAH, data herein demonstrate that exosomes promote flux into the TCA cycle, resulting in elevated oxidative phosphorylation. We provide evidence that exosomes promote anaplerosis through the expression of PDH and GLUD1. Furthermore, we demonstrate that exosomes inhibit SIRT4 expression and suggest that curbing SIRT4, upstream of PDH and GLUD1, contributes to the exosome-mediated improvement in mitochondrial function. Taken together, our results suggest that exosome treatment improves mitochondrial function by jumpstarting the TCA cycle through provision of nutrients.

PAH is associated with decreased mitochondrial function, an underlying perturbation contributing to disease (1, 5, 66). Commonly, animal models use prolonged hypoxia to induce remodeling of the vascular smooth muscle, leading to chronic vasoconstriction and hyperplasia of vascular smooth muscle cells, as seen in PAH (58). Importantly, this hypoxia exposure results in mitochondrial perturbations consistent with those seen in patients with PAH (8). In an effort to capture this phenotype in vitro, we exposed human PASMCs to low oxygen for 2 wk. Consistent with patients with PAH, the prolonged hypoxia regimen resulted in hyperproliferation of PASMCs (data not shown), elevated lactate production, and decreased metabolite entry into the TCA cycle (Fig. 2). These data support the use of chronic hypoxia as a model of PAH-associated mitochondrial dysfunction. Importantly, exosome treatment rescued the effects of hypoxia exposure, decreasing lactate production and increasing TCA cycle metabolites. Furthermore, providing definitive evidence of rescued mitochondrial function, exosome treatment increased oxygen consumption after hypoxia exposure in a dose-dependent manner (Fig. 2*F*). These data were confirmed using a semaxanib/hypoxia rat model of PAH. Exosomes increased TCA cycle metabolites and decreased polyol pathway metabolites in semaxanib/hyp-

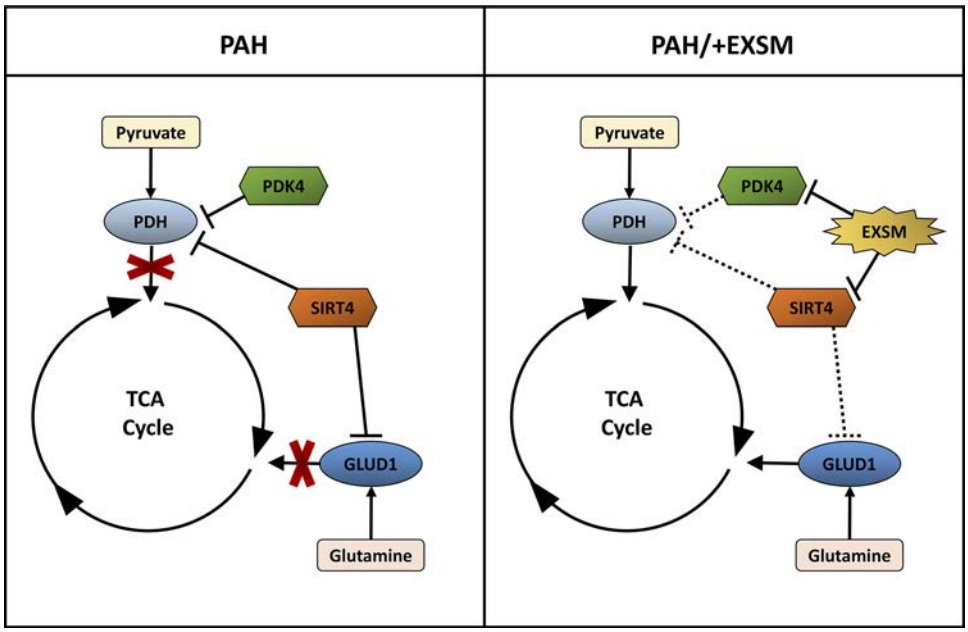

Fig. 9. Proposed exosome mechanism of action targets sirtuin 4 (SIRT4) in pulmonary arterial hypertension (PAH). We propose that chronic hypoxia in pulmonary artery smooth muscle cells inhibits TCA cycle function by upregulating SIRT4, which inhibits pyruvate dehydrogenase (PDH) and glutamate dehydrogenase 1 (GLUD1) and limits pyruvate and glutamine entry into the TCA cycle (*left*). Exosome treatment downregulates SIRT4, thereby increasing glutamine and pyruvate flux into the TCA cycle (*right*). EXSM, exosome; PDK4, pyruvate dehydrogenase kinase 4.

oxia tissue, indicative of an elevation in oxidative phosphorylation (Fig. 4) (11, 27, 48).

The concept of extracellular vesicles containing mitochondrial components, such as mitochondrial proteins and mRNA, is not new. In fact, intracellular mitochondrial transfer has been shown by multiple groups (reviewed in Ref. 60). In these studies, vesicles have been suggested to participate in horizontal transfer of intact mitochondria, leading to improvements in mitochondrial function (53). However, herein exosomes generated from bone marrow MSCs are not able to consume oxygen (data not shown), indicating the lack of an intact electron transport chain. Additionally, the use of size exclusion chromatography to isolate exosomes herein results in particles in the 50-nm to 200-nm size range (Fig. 1), whereas intact mitochondria range from 0.5 to 10 μm. Therefore, the potential transfer of intact mitochondria is unlikely to cause the observed improvements in mitochondrial dysfunction. We and others have shown that exosomes contain mitochondrial proteins, mtDNA, and mitochondrial genes (19, 30, 62). We propose the transfer of this mitochondrial protein and genetic material functions to boost mitochondrial function via host cell remodeling. With this in mind, we sought to determine the mechanism by which exosomes improve oxidative phosphorylation.

Mapping of metabolite entry into the TCA cycle resulted in a clear exosome-mediated induction of two distinct entry points, glutamate and pyruvate (Fig. 5). These data suggest a potential regulation of key enzymes within these pathways. GLUD1 converts glutamate to the TCA cycle metabolite, α-ketoglutarate. Shown to be inhibited in severe hypoxia and an in vitro model of PAH, a decrease in GLUD1 activity is consistent with the decline in TCA cycle function in PAH (7, 14, 16, 24). Herein we show that chronic hypoxia results in a deficit in GLUD1, both at the gene and protein levels (Figs. 6 and 7). Exosome exposure rescued mRNA and protein expression of GLUD1 in parallel with heightened TCA cycle metabolites, indicative of increased nutrient flow into the TCA cycle.

PDH converts pyruvate into acetyl-CoA, linking glycolysis to the TCA cycle. PDH consists of four enzymatic components that are highly regulated: pyruvate dehydrogenase (E1), dihydrolipoamide acetyltransferase (E2), lipoamide dehydrogenase (E3), and E3-binding protein (17, 43). Composed of a heterotetramer of two α- and two β-subunits, the E1α site is specifically inhibited through phosphorylation by PDK4 (29). Importantly, elevations in PDK4 protein and diminished PDH activity are common in patients with PAH (47). In agreement with previous studies, we show a hypoxia-mediated increase in PDK4 gene and protein levels and a subsequent decline in PDH, consistent with PAH (31). Interestingly, exosomes induce PDH gene expression through E1 subunit β and via inhibition of PDK (Fig. 6). These data suggest the potential of exosomes to modulate both subunits in the E1 enzyme (E1α through inhibition of PDK4 and E1β through direct induction of gene expression). Redundant activation in this way may be required to fully improve flux through the PDH complex, though further work is required to explore this possibility. Beyond increases in PDH gene regulation, Fig. 7 demonstrates a dose-responsive regulation of PDH and PDK4 proteins, highly suggestive of an exosome-mediated restoration of PDH in the context of mitochondrial dysfunction.

We hypothesize that increased flux through GLUD1 and PDH might be sufficient to increase mitochondrial function. This hypothesis is supported by experiments examining dichloroacetate, a PDK inhibitor, as a potential therapeutic for metabolic dysfunction in PAH (20, 32). Dichloroacetate studies propose that increased PDH activity alone could benefit patients with PAH. Herein, we suggest that the increase in flux through both PDH and GLUD1 make exosomes an exciting therapeutic strategy for combating the metabolic dysfunction associated with PAH. Exosomes have proven effective in treating other aspects of the disease, including peripheral pulmonary arteriolar remodeling and lung inflammation (22, 31). Therefore, exosomes could provide a multifaceted treatment for PAH, improving vascular remodeling and the underlying metabolic disorder in disease.

Lastly, results herein describe the possible involvement of SIRT4 in the pathogenesis of PAH. Known to function as an

ADP-ribosyltransferase, much work is still needed to fully understand the role of SIRT4 in the mitochondria. Previous studies have shown that genetic inhibition of SIRT4 increased oxygen consumption (25, 40). Furthermore, SIRT4 prevented hypoxia-induced apoptosis after acute hypoxia exposure (35). Given that SIRT4 has been shown to inhibit GLUD1 and PDH, perhaps SIRT4 protects against hypoxia-induced cell death by reducing metabolite entry into the TCA cycle via these two nutrient entry points (21, 38). However, SIRT4 may become chronically activated after prolonged hypoxia, contributing to mitochondrial dysfunction. In support of this hypothesis, we demonstrate an increase in SIRT4 gene expression with increased hypoxia exposure (Fig. 8*A*). Exosome treatment reduced SIRT4 gene expression, even at low treatment volume (Fig. 8*B*), tempting speculation that exosomes could play a role in SIRT4 regulation. Further work is needed to fully tease apart the role of SIRT4 in PAH and potential exosome-mediated inhibition of this enzyme.

ACKNOWLEDGMENTS

We thank collaborators at the Stella Kourembanas laboratory in the Boston Children's Hospital and the Regenerative Medicine Laboratory members at United Therapeutics for support in this study.

DISCLOSURES

No conflicts of interest, financial or otherwise, are declared by the authors.

AUTHOR CONTRIBUTIONS

S.E.H. and M.P.R.S. conceived and designed research; S.E.H., M.P.R.S., R.G., and C.M. performed experiments; S.E.H., M.P.R.S., J.C., and C.M. analyzed data; S.E.H., M.P.R.S., J.C., and R.M.I. interpreted results of experiments; S.E.H., M.P.R.S., and J.C. prepared figures; S.E.H. and M.P.R.S. drafted manuscript; S.E.H., M.P.R.S., T.H.P., and R.M.I. edited and revised manuscript; S.E.H., M.P.R.S., J.C., R.G., C.M., T.H.P., and R.M.I. approved final version of manuscript.

REFERENCES

1. **Abernethy AD, Stackhouse K, Hart S, Devendra G, Bashore TM, Dweik R, Krasuski RA.** Impact of diabetes in patients with pulmonary hypertension. *Pulm Circ* 5: 117–123, 2015. doi:10.1086/679705.
2. **Aliotta JM, Pereira M, Wen S, Dooner MS, Del Tatto M, Papa E, Goldberg LR, Baird GL, Ventetuolo CE, Quesenberry PJ, Klinger JR.** Exosomes induce and reverse monocrotaline-induced pulmonary hypertension in mice. *Cardiovasc Res* 110: 319–330, 2016. doi:10.1093/cvr/cvw054.
3. **Archer SL, Gomberg-Maitland M, Maitland ML, Rich S, Garcia JG, Weir EK.** Mitochondrial metabolism, redox signaling, and fusion: a mitochondria-ROS-HIF-1α-Kv1.5 O2-sensing pathway at the intersection of pulmonary hypertension and cancer. *Am J Physiol Heart Circ Physiol* 294: H570–H578, 2008. doi:10.1152/ajpheart.01324.2007.
4. **Assad TR, Hemnes AR.** Metabolic dysfunction in pulmonary arterial hypertension. *Curr Hypertens Rep* 17: 20, 2015. doi:10.1007/s11906-014-0524-y.
5. **Benson L, Brittain EL, Pugh ME, Austin ED, Fox K, Wheeler L, Robbins IM, Hemnes AR.** Impact of diabetes on survival and right ventricular compensation in pulmonary arterial hypertension. *Pulm Circ* 4: 311–318, 2014. doi:10.1086/675994.
6. **Bhat L, Hawkinson J, Cantillon M, Reddy DG, Bhat SR, Laurent CE, Bouchard A, Biernat M, Salvail D.** RP5063, a novel, multimodal, serotonin receptor modulator, prevents Sugen 5416-hypoxia-induced pulmonary arterial hypertension in rats. *Eur J Pharmacol* 810: 83–91, 2017. doi:10.1016/j.ejphar.2017.05.052.
7. **Boehme J, Sun X, Tormos KV, Gong W, Kellner M, Datar SA, Kameny RJ, Yuan JX, Raff GW, Fineman JR, Black SM, Maltepe E.** Pulmonary artery smooth muscle cell hyperproliferation and metabolic shift triggered by pulmonary overcirculation. *Am J Physiol Heart Circ Physiol* 311: H944–H957, 2016. doi:10.1152/ajpheart.00040.2016.
8. **Bonnet S, Michelakis ED, Porter CJ, Andrade-Navarro MA, Thébaud B, Bonnet S, Haromy A, Harry G, Moudgil R, McMurtry MS, Weir EK, Archer SL.** An abnormal mitochondrial-hypoxia inducible factor-1alpha-Kv channel pathway disrupts oxygen sensing and triggers pulmonary arterial hypertension in fawn hooded rats: similarities to human pulmonary arterial hypertension. *Circulation* 113: 2630–2641, 2006. doi:10.1161/CIRCULATIONAHA.105.609008.
9. **Bonnet S, Provencher S, Guignabert C, Perros F, Boucherat O, Schermuly RT, Hassoun PM, Rabinovitch M, Nicolls MR, Humbert M.** Translating research into improved patient care in pulmonary arterial hypertension. *Am J Respir Crit Care Med* 195: 583–595, 2017. doi:10.1164/rccm.201607-1515PP.
10. **Boucherat O, Peterlini T, Bourgeois A, Nadeau V, Breuils-Bonnet S, Boilet-Molez S, Potus F, Meloche J, Chabot S, Lambert C, Tremblay E, Chae YC, Altieri DC, Sutendra G, Michelakis ED, Paulin R, Provencher S, Bonnet S.** Mitochondrial HSP90 accumulation promotes vascular remodeling in pulmonary arterial hypertension. *Am J Respir Crit Care Med* 198: 90–103, 2018. doi:10.1164/rccm.201708-1751OC.
11. **Cameron NE, Cotter MA, Robertson S.** Contractile properties of cardiac papillary muscle in streptozotocin-diabetic rats and the effects of aldose reductase inhibition. *Diabetologia* 32: 365–370, 1989. doi:10.1007/BF00277260.
12. **Chettimada S, Gupte R, Rawat D, Gebb SA, McMurtry IF, Gupte SA.** Hypoxia-induced glucose-6-phosphate dehydrogenase overexpression and -activation in pulmonary artery smooth muscle cells: implication in pulmonary hypertension. *Am J Physiol Lung Cell Mol Physiol* 308: L287–L300, 2015. doi:10.1152/ajplung.00229.2014.
13. **Cottrill KA, Chan SY.** Metabolic dysfunction in pulmonary hypertension: the expanding relevance of the Warburg effect. *Eur J Clin Invest* 43: 855–865, 2013. doi:10.1111/eci.12104.
14. **Dawson NJ, Storey KB.** An enzymatic bridge between carbohydrate and amino acid metabolism: regulation of glutamate dehydrogenase by reversible phosphorylation in a severe hypoxia-tolerant crayfish. *J Comp Physiol B* 182: 331–340, 2012. doi:10.1007/s00360-011-0629-4.
15. **Doucet-Beaupré H, Gilbert C, Profes MS, Chabrat A, Pacelli C, Giguère N, Rioux V, Charest J, Deng Q, Laguna A, Ericson J, Perlmann T, Ang SL, Cicchetti F, Parent M, Trudeau LE, Lévesque M.** Lmx1a and Lmx1b regulate mitochondrial functions and survival of adult midbrain dopaminergic neurons. *Proc Natl Acad Sci USA* 113: E4387–E4396, 2016. doi:10.1073/pnas.1520387113.
16. **Fessel JP, Hamid R, Wittmann BM, Robinson LJ, Blackwell T, Tada Y, Tanabe N, Tatsumi K, Hemnes AR, West JD.** Metabolomic analysis of bone morphogenetic protein receptor type 2 mutations in human pulmonary endothelium reveals widespread metabolic reprogramming. *Pulm Circ* 2: 201–213, 2012. doi:10.4103/2045-8932.97606.
17. **Gray LR, Tompkins SC, Taylor EB.** Regulation of pyruvate metabolism and human disease. *Cell Mol Life Sci* 71: 2577–2604, 2014. doi:10.1007/s00018-013-1539-2.
18. **Groth A, Vrugt B, Brock M, Speich R, Ulrich S, Huber LC.** Inflammatory cytokines in pulmonary hypertension. *Respir Res* 15: 47, 2014. doi:10.1186/1465-9921-15-47.
19. **Guescini M, Guidolin D, Vallorani L, Casadei L, Gioacchini AM, Tibollo P, Battistelli M, Falcieri E, Battistin L, Agnati LF, Stocchi V.** C2C12 myoblasts release micro-vesicles containing mtDNA and proteins involved in signal transduction. *Exp Cell Res* 316: 1977–1984, 2010. doi:10.1016/j.yexcr.2010.04.006.
20. **Guignabert C, Tu L, Izikki M, Dewachter L, Zadigue P, Humbert M, Adnot S, Fadel E, Eddahibi S.** Dichloroacetate treatment partially regresses established pulmonary hypertension in mice with SM22alpha-targeted overexpression of the serotonin transporter. *FASEB J* 23: 4135–4147, 2009. doi:10.1096/fj.09-131664.
21. **Haigis MC, Mostoslavsky R, Haigis KM, Fahie K, Christodoulou DC, Murphy AJ, Valenzuela DM, Yancopoulos GD, Karow M, Blander G, Wolberger C, Prolla TA, Weindruch R, Alt FW, Guarente L.** SIRT4 inhibits glutamate dehydrogenase and opposes the effects of calorie restriction in pancreatic beta cells. *Cell* 126: 941–954, 2006. doi:10.1016/j.cell.2006.06.057.
22. **Hansmann G, Fernandez-Gonzalez A, Aslam M, Vitali SH, Martin T, Mitsialis SA, Kourembanas S.** Mesenchymal stem cell-mediated reversal of bronchopulmonary dysplasia and associated pulmonary hypertension. *Pulm Circ* 2: 170–181, 2012. doi:10.4103/2045-8932.97603.
23. **Harvey LD, Chan SY.** Emerging metabolic therapies in pulmonary arterial hypertension. *J Clin Med* 6: 43, 2017. doi:10.3390/jcm6040043.

24. **Hemnes AR, Brittain EL, Trammell AW, Fessel JP, Austin ED, Penner N, Maynard KB, Gleaves L, Talati M, Absi T, Disalvo T, West J.** Evidence for right ventricular lipotoxicity in heritable pulmonary arterial hypertension. *Am J Respir Crit Care Med* 189: 325–334, 2014. doi:10.1164/rccm.201306-1086OC.
25. **Ho L, Titus AS, Banerjee KK, George S, Lin W, Deota S, Saha AK, Nakamura K, Gut P, Verdin E, Kolthur-Seetharam U.** SIRT4 regulates ATP homeostasis and mediates a retrograde signaling via AMPK. *Aging (Albany NY)* 5: 835–849, 2013. doi:10.18632/aging.100616.
26. **Jacquin S, Rincheval V, Mignotte B, Richard S, Humbert M, Mercier O, Londoño-Vallejo A, Fadel E, Eddahibi S.** Inactivation of p53 is sufficient to induce development of pulmonary hypertension in rats. *PLoS One* 10: e0131940, 2015. doi:10.1371/journal.pone.0131940.
27. **Kashiwagi A, Obata T, Suzaki M, Takagi Y, Kida Y, Ogawa T, Tanaka Y, Asahina T, Ikebuchi M, Saeki Y, Kikkawa R, Shigeta Y.** Increase in cardiac muscle fructose content in streptozotocin-induced diabetic rats. *Metabolism* 41: 1041–1046, 1992. doi:10.1016/0026-0495(92)90283-G.
28. **Komanduri KV, Couriel D, Champlin RE.** Graft-versus-host disease after allogeneic stem cell transplantation: evolving concepts and novel therapies including photopheresis. *Biol Blood Marrow Transplant* 12, *Suppl* 2: 1–6, 2006. doi:10.1016/j.bbmt.2005.11.003.
29. **Korotchkina LG, Patel MS.** Site specificity of four pyruvate dehydrogenase kinase isoenzymes toward the three phosphorylation sites of human pyruvate dehydrogenase. *J Biol Chem* 276: 37223–37229, 2001. doi:10.1074/jbc.M103069200.
30. **Kowal J, Arras G, Colombo M, Jouve M, Morath JP, Primdal-Bengtson B, Dingli F, Loew D, Tkach M, Théry C.** Proteomic comparison defines novel markers to characterize heterogeneous populations of extracellular vesicle subtypes. *Proc Natl Acad Sci USA* 113: E968–E977, 2016. doi:10.1073/pnas.1521230113.
31. **Lee C, Mitsialis SA, Aslam M, Vitali SH, Vergadi E, Konstantinou G, Sdrimas K, Fernandez-Gonzalez A, Kourembanas S.** Exosomes mediate the cytoprotective action of mesenchymal stromal cells on hypoxia-induced pulmonary hypertension. *Circulation* 126: 2601–2611, 2012. doi:10.1161/CIRCULATIONAHA.112.114173.
32. **Li B, Yan J, Shen Y, Liu Y, Ma Z.** Dichloroacetate prevents but not reverses the formation of neointimal lesions in a rat model of severe pulmonary arterial hypertension. *Mol Med Rep* 10: 2144–2152, 2014. doi:10.3892/mmr.2014.2432.
33. **Li MX, Jiang DQ, Wang Y, Chen QZ, Ma YJ, Yu SS, Wang Y.** Signal mechanisms of vascular remodeling in the development of pulmonary arterial hypertension. *J Cardiovasc Pharmacol* 67: 182–190, 2016. doi:10.1097/FJC.0000000000000328.
34. **Li Y, Park JS, Deng JH, Bai Y.** Cytochrome c oxidase subunit IV is essential for assembly and respiratory function of the enzyme complex. *J Bioenerg Biomembr* 38: 283–291, 2006. doi:10.1007/s10863-006-9052-z.
35. **Liu B, Che W, Xue J, Zheng C, Tang K, Zhang J, Wen J, Xu Y.** SIRT4 prevents hypoxia-induced apoptosis in H9c2 cardiomyoblast cells. *Cell Physiol Biochem* 32: 655–662, 2013. doi:10.1159/000354469.
36. **Mariappan N, Elks CM, Fink B, Francis J.** TNF-induced mitochondrial damage: a link between mitochondrial complex I activity and left ventricular dysfunction. *Free Radic Biol Med* 46: 462–470, 2009. doi:10.1016/j.freeradbiomed.2008.10.049.
37. **Marsboom G, Wietholt C, Haney CR, Toth PT, Ryan JJ, Morrow E, Thenappan T, Bache-Wiig P, Piao L, Paul J, Chen CT, Archer SL.** Lung ^{18}F-fluorodeoxyglucose positron emission tomography for diagnosis and monitoring of pulmonary arterial hypertension. *Am J Respir Crit Care Med* 185: 670–679, 2012. doi:10.1164/rccm.201108-1562OC.
38. **Mathias RA, Greco TM, Oberstein A, Budayeva HG, Chakrabarti R, Rowland EA, Kang Y, Shenk T, Cristea IM.** Sirtuin 4 is a lipoamidase regulating pyruvate dehydrogenase complex activity. *Cell* 159: 1615–1625, 2014. doi:10.1016/j.cell.2014.11.046.
39. **Moreira-Gonçalves D, Padrão AI, Ferreira R, Justino J, Nogueira-Ferreira R, Neuparth MJ, Vitorino R, Fonseca H, Silva AF, Duarte JA, Leite-Moreira A, Henriques-Coelho T.** Signaling pathways underlying skeletal muscle wasting in experimental pulmonary arterial hypertension. *Biochim Biophys Acta* 1852: 2722–2731, 2015. doi:10.1016/j.bbadis.2015.10.002.
40. **Nasrin N, Wu X, Fortier E, Feng Y, Bare' OC, Chen S, Ren X, Wu Z, Streeper RS, Bordone L.** SIRT4 regulates fatty acid oxidation and mitochondrial gene expression in liver and muscle cells. *J Biol Chem* 285: 31995–32002, 2010. doi:10.1074/jbc.M110.124164.
41. **Nogueira-Ferreira R, Ferreira R, Henriques-Coelho T.** Cellular interplay in pulmonary arterial hypertension: implications for new therapies. *Biochim Biophys Acta* 1843: 885–893, 2014. doi:10.1016/j.bbamcr.2014.01.030.
42. **Parra V, Bravo-Sagua R, Norambuena-Soto I, Hernández-Fuentes CP, Gómez-Contreras AG, Verdejo HE, Mellado R, Chiong M, Lavandero S, Castro PF.** Inhibition of mitochondrial fission prevents hypoxia-induced metabolic shift and cellular proliferation of pulmonary arterial smooth muscle cells. *Biochim Biophys Acta Mol Basis Dis* 1863: 2891–2903, 2017. doi:10.1016/j.bbadis.2017.07.018.
43. **Patel MS, Korotchkina LG, Sidhu S.** Interaction of E1 and E3 components with the core proteins of the human pyruvate dehydrogenase complex. *J Mol Catal, B Enzym* 61: 2–6, 2009. doi:10.1016/j.molcatb.2009.05.001.
44. **Paulin R, Michelakis ED.** The metabolic theory of pulmonary arterial hypertension. *Circ Res* 115: 148–164, 2014. doi:10.1161/CIRCRESAHA.115.301130.
45. **Peng H, Xiao Y, Deng X, Luo J, Hong C, Qin X.** The Warburg effect: a new story in pulmonary arterial hypertension. *Clin Chim Acta* 461: 53–58, 2016. doi:10.1016/j.cca.2016.07.017.
46. **Phinney DG, Di Giuseppe M, Njah J, Sala E, Shiva S, St Croix CM, Stolz DB, Watkins SC, Di YP, Leikauf GD, Kolls J, Riches DW, Deiuliis G, Kaminski N, Boregowda SV, McKenna DH, Ortiz LA.** Mesenchymal stem cells use extracellular vesicles to outsource mitophagy and shuttle microRNAs. *Nat Commun* 6: 8472, 2015. doi:10.1038/ncomms9472.
47. **Piao L, Sidhu VK, Fang YH, Ryan JJ, Parikh KS, Hong Z, Toth PT, Morrow E, Kutty S, Lopaschuk GD, Archer SL.** FOXO1-mediated upregulation of pyruvate dehydrogenase kinase-4 (PDK4) decreases glucose oxidation and impairs right ventricular function in pulmonary hypertension: therapeutic benefits of dichloroacetate. *J Mol Med (Berl)* 91: 333–346, 2013. doi:10.1007/s00109-012-0982-0.
48. **Poulsom R, Boot-Handford RP, Heath H.** The effects of long-term treatment of streptozotocin-diabetic rats with an aldose reductase inhibitor. *Exp Eye Res* 37: 507–515, 1983. doi:10.1016/0014-4835(83)90027-1.
49. **Rafikov R, Sun X, Rafikova O, Meadows ML, Desai AA, Khalpey Z, Yuan JX, Fineman JR, Black SM.** Complex I dysfunction underlies the glycolytic switch in pulmonary hypertensive smooth muscle cells. *Redox Biol* 6: 278–286, 2015. doi:10.1016/j.redox.2015.07.016.
50. **Raghavan A, Zhou G, Zhou Q, Ibe JC, Ramchandran R, Yang Q, Racherla H, Raychaudhuri P, Raj JU.** Hypoxia-induced pulmonary arterial smooth muscle cell proliferation is controlled by forkhead box M1. *Am J Respir Cell Mol Biol* 46: 431–436, 2012. doi:10.1165/rcmb.2011-0128OC.
51. **Rehman J, Archer SL.** A proposed mitochondrial-metabolic mechanism for initiation and maintenance of pulmonary arterial hypertension in fawn-hooded rats: the Warburg model of pulmonary arterial hypertension. *Adv Exp Med Biol* 661: 171–185, 2010. doi:10.1007/978-1-60761-500-2_11.
52. **Shimoda LA, Laurie SS.** Vascular remodeling in pulmonary hypertension. *J Mol Med (Berl)* 91: 297–309, 2013. doi:10.1007/s00109-013-0998-0.
53. **Spees JL, Olson SD, Whitney MJ, Prockop DJ.** Mitochondrial transfer between cells can rescue aerobic respiration. *Proc Natl Acad Sci USA* 103: 1283–1288, 2006. doi:10.1073/pnas.0510511103.
54. **Suen C, Mei SH, Stewart DJ.** Cell therapy for PAH: potential efficacy of endothelial progenitor cells and mesenchymal stem cells. *Adv Pulm Hypertens* 11: 33–38, 2012.
55. **Sun RC, Denko NC.** Hypoxic regulation of glutamine metabolism through HIF1 and SIAH2 supports lipid synthesis that is necessary for tumor growth. *Cell Metab* 19: 285–292, 2014. doi:10.1016/j.cmet.2013.11.022.
56. **Sutendra G, Michelakis ED.** The metabolic basis of pulmonary arterial hypertension. *Cell Metab* 19: 558–573, 2014. doi:10.1016/j.cmet.2014.01.004.
58. **Sztuka K, Jasińska-Stroschein M.** Animal models of pulmonary arterial hypertension: A systematic review and meta-analysis of data from 6126 animals. *Pharmacol Res* 125: 201–214, 2017. doi:10.1016/j.phrs.2017.08.003.
59. **Taraseviciene-Stewart L, Kasahara Y, Alger L, Hirth P, Mc Mahon G, Waltenberger J, Voelkel NF, Tuder RM.** Inhibition of the VEGF receptor 2 combined with chronic hypoxia causes cell death-dependent pulmonary endothelial cell proliferation and severe pulmonary hypertension. *FASEB J* 15: 427–438, 2001. doi:10.1096/fj.00-0343com.
60. **Torralba D, Baixauli F, Sánchez-Madrid F.** Mitochondria know no boundaries: mechanisms and functions of intercellular mitochondrial transfer. *Front Cell Dev Biol* 4: 107, 2016. doi:10.3389/fcell.2016.00107.

61. **Usselman RJ, Chavarriaga C, Castello PR, Procopio M, Ritz T, Dratz EA, Singel DJ, Martino CF.** The quantum biology of reactive oxygen species partitioning impacts cellular bioenergetics. *Sci Rep* 6: 38543, 2016. doi:10.1038/srep38543.
62. **van Balkom BW, Eisele AS, Pegtel DM, Bervoets S, Verhaar MC.** Quantitative and qualitative analysis of small RNAs in human endothelial cells and exosomes provides insights into localized RNA processing, degradation and sorting. *J Extracell Vesicles* 4: 26760, 2015. doi:10.3402/jev.v4.26760.
63. **Wang H, Ao M, Wu J, Yu L.** TNFα and Fas/FasL pathways are involved in 9-Methoxycamptothecin-induced apoptosis in cancer cells with oxidative stress and G2/M cell cycle arrest. *Food Chem Toxicol* 55: 396–410, 2013. doi:10.1016/j.fct.2012.12.059.
64. **Yu B, Zhang X, Li X.** Exosomes derived from mesenchymal stem cells. *Int J Mol Sci* 15: 4142–4157, 2014. doi:10.3390/ijms15034142.
65. **Yuan K, Shao NY, Hennigs JK, Discipulo M, Orcholski ME, Shamskhou E, Richter A, Hu X, Wu JC, de Jesus Perez VA.** Increased pyruvate dehydrogenase kinase 4 expression in lung pericytes is associated with reduced endothelial-pericyte interactions and small vessel loss in pulmonary arterial hypertension. *Am J Pathol* 186: 2500–2514, 2016. doi:10.1016/j.ajpath.2016.05.016.
66. **Zamanian RT, Hansmann G, Snook S, Lilienfeld D, Rappaport KM, Reaven GM, Rabinovitch M, Doyle RL.** Insulin resistance in pulmonary arterial hypertension. *Eur Respir J* 33: 318–324, 2009. doi:10.1183/09031936.00000508.
67. **Zhao Y, Peng J, Lu C, Hsin M, Mura M, Wu L, Chu L, Zamel R, Machuca T, Waddell T, Liu M, Keshavjee S, Granton J, de Perrot M.** Metabolomic heterogeneity of pulmonary arterial hypertension. *PLoS One* 9: e88727, 2014. doi:10.1371/journal.pone.0088727.
68. **Zitka O, Skalickova S, Gumulec J, Masarik M, Adam V, Hubalek J, Trnkova L, Kruseova J, Eckschlager T, Kizek R.** Redox status expressed as GSH:GSSG ratio as a marker for oxidative stress in paediatric tumour patients. *Oncol Lett* 4: 1247–1253, 2012. doi:10.3892/ol.2012.931.